

**FUNCTIONAL ELEMENTS WITHIN CARD11'S INHIBITORY  
DOMAIN DICTATE DOWNSTREAM SIGNALING TO NF-KAPPA B  
IN LYMPHOCYTES**

By  
Rakhi P. Jattani

A dissertation submitted to Johns Hopkins University in conformity with the  
requirements for the degree of Doctor of Philosophy

Baltimore, Maryland  
December, 2014

## **Abstract**

Antigen (Ag) receptor engagement on lymphocytes triggers a signaling cascade that phosphorylates the scaffold protein CARD11 in its inhibitory domain (ID) and transforms it from a closed and inactive state into an open and active conformation. This conformational change results in disruption of intramolecular interactions, cofactor assembly, NF- $\kappa$ B activation and lymphocyte activation. To better understand how CARD11's inhibitory domain regulates these functions, we performed a systematic analysis of the 231 residues that comprise the inhibitory domain. We discovered the inhibitory domain is made up of multiple operational elements that cooperatively control its overall function. Four independent and redundant repressive elements maintain CARD11 in the closed conformation and prevent Bcl10 association. A single, contiguous inducibility element controls the transition from the closed to open conformation. Furthermore, we identified two novel activating elements that demonstrated a greater potential for CARD11 hyperactivity than was previously thought. We found that lymphoma-associated mutations in CARD11 disrupted intramolecular binding to multiple repressive elements, allowing them to bypass the need for inhibitory domain phosphorylation. Overall, we uncovered a highly evolved mechanism of modulating CARD11's inhibitory domain that precisely tunes NF- $\kappa$ B levels and lymphocyte function.

## **Ph.D. DISSERTATION REFEREES**

Joel L. Pomerantz, Ph.D. (faculty sponsor)

Associate Professor, Biological Chemistry

Johns Hopkins University School of Medicine

Edward W. Harhaj, B.A., Ph.D. (reader)

Associate Professor, Department of Oncology

Johns Hopkins School of Medicine

Sidney Kimmel Comprehensive Cancer Center

## **Acknowledgements**

I would first and foremost like to thank my advisor Joel Pomerantz. He accepted me into his lab when I knew only the basics of immunology and biochemistry. Not only was he patient and supportive of my exploration into these new fields of study, but he taught me how to think like a scientist. His encouragement, dedication and scientific rigor pushed me to be a better scientist.

For all their many years of input and advice, I would also like to thank my thesis committee members Stephen Desiderio, Robert Silicano, Edward Harhaj, Mike Matunis and Craig Montell. Dan Raben was helpful in the last two years acting as the BCMB Policy member who made sure my project was progressing in a timely manner. I extend an extra thanks to Ed for agreeing to be my thesis reader.

I would also like to thank all the current and past members of the Pomerantz lab. I am a much better scientist because of their willingness to teach me, share their experiences and give me scientific advice. Valerie Schowinsky and Becky Lamason especially took me under their wings, teaching me new techniques and bestowing their knowledge onto me without hesitation any time I asked. I am thankful to Ryan McCully and Waipan Chan whose work laid the groundwork for my thesis project and made my job that much easier. I am indebted to Julia Tritapoe, who for the last three years, has been instrumental in helping me move this project forward. No matter what help I needed in or outside of lab, she was always there offering her assistance with a smile. Along with Julia, Zhaoquan Wang and Stefanie Lew have been like my family in lab, supporting me

scientifically, professionally and personally. No matter what was happening scientifically, they made sure that every day was interesting and that there was always something I could appreciate that day. I also need to thank several Pomrantz rotation students who helped me with various parts of my project, including Deidre Ribbens, Corinne Hamblet, Sarah Pedersen, Hong Sun, Phillip Wulfridge, Eric Schiffhauer and Jaime Wengen.

I am lucky to have made some lifelong friends in graduate school. Qing Huang, Edel Hyland and Lisa Huang helped ease the pains of graduate school. They always reminded me of the bright side of things and that I always had their company to look forward to.

I would like to thank my boyfriend, Robert Yarrington. He has been my lifeline throughout my graduate career. He carried me through all the highs and lows and, together, we come out on top. No matter what happened in lab, I knew I had one constant in my life. I could always count on his unconditional love and support.

Finally, I could not have made it through graduate school without my family. My dad taught me the importance of working hard and never giving up. My grandmother's strength and courage in the face of adversity inspired me to keep pushing forward. Throughout the years, my dad and sister always believed in me, knowing I am capable of more than I thought I was. I will forever be thankful for their encouragement and support.

## Table of Contents

Title Page	i
Abstract	ii
Acknowledgements	iv
Table of Contents	vi
List of Tables	viii
List of Figures	ix
Chapter I: Introduction	1
Chapter II: Functional elements in CARD11's inhibitory domain modulate NF-kappaB activity	5
CARD11's Inhibitory Domain contains multiple, redundant Repressive Elements	6
CARD11's Inhibitory Domain contains two independent Activating Elements	9
CARD11's Inhibitory Domain contains a single Inducibility Element	10
CARD11's Repressive Elements require multiple mutations to abolish RE function	11
CARD11's Repressive Elements cooperate to repress downstream signaling to NF-κB	12
Bcl10 association is regulated by multiple Repressive Elements	13

CARD11's Repressive Elements synergize to control intramolecular binding	14
Repressive Elements bind differential CARD11 intramolecular targets	15
Lymphoma-associated, gain-of-function CARD11 mutations disrupt binding of at least two Repressive Elements	16
Experimental Procedures	17
Tables	21
Figures and Figure Legends	31
Chapter III: Discussion	71
References	80
Curriculum Vitae	88

## **List of Tables**

Table 2.1: CARD11 deletion and mutant constructs

Table 2.2: CARD11 mutant primers and oligo

Table 2.3: CARD11 full-length mutant constructs

Table 2.4: Relative activities of CARD11 full-length RE mutants



## List of Figures

Figure 2.1: CARD11's inhibitory domain comprises of multiple functional elements

Figure 2.2: CARD11's inhibitory function consists of multiple regions with repressive function

Figure 2.3: N-terminus of ID contains a repressive element

Figure 2.4: CARD11 RE1 maps to residues 441-493

Figure 2.5: C-terminus of ID contains a novel activating element and a potent repressive element.

Figure 2.6: CARD11 RE4 maps to residues 617-641

Figure 2.7: M1 and M2 abolish RE1 repressive function

Figure 2.8: Multiple mutations in RE4 disrupt its repression

Figure 2.9: Internal regions of the ID include at least one additional repressive element

Figure 2.10: CARD11 RE2 and RE3 share homologous sequences that abrogate repression when mutated

Figure 2.11: CARD11 ID encodes a second activating element

Figure 2.12: CARD11's inducibility element is embedded within activating element1

Figure 2.13: Multiple mutations in multiple repressive elements are required to completely destroy inhibitory function

Figure 2.14: Repressive elements act synergistically to repressive basal NF- $\kappa$ B activity

Figure 2.15: All repressive elements work together to prevent Bcl10 association

Figure 2.16: Multiple repressive elements control intramolecular binding

Figure 2.17: Isolated repressive elements are sufficient to bind to other domains within CARD11

Figure 2.18: Repressive elements 1, 2 and 3 bind to different domains of CARD11

Figure 2.19: Oncogenic CARD11 mutations disrupt binding to multiple ID repressive elements

## **Chapter I: Introduction**

The precise and rapid activation of NF- $\kappa$ B activation downstream of antigen receptor engagement is important to mount an anti-inflammatory response in T cells and B cells (Schulze-Luehrmann and Ghosh, 2006; Wegener and Krappmann, 2007). Central to the activation of T cell receptor (TCR) or B cell receptor (BCR) signaling to NF- $\kappa$ B is the adaptor molecule caspase-recruitment domain 11 (CARD11) (Egawa et al., 2003; Gaide et al., 2002; Jun et al., 2003; Pomerantz et al., 2002; Wang et al., 2002). CARD11 is a multi-domain scaffold protein, consisting of an N-terminal CARD domain, followed by a linker (L1), coiled-coiled domain (CC), an inhibitory domain (ID), PDZ domain, another linker (L3), SH3 domain, an additional linker (L4) and a guanylate kinase domain (GUK). Upon TCR engagement, membrane proximal kinases initiate a signaling cascade that activates protein kinase C  $\theta$  (PKC $\theta$ ), which phosphorylates CARD11 in its inhibitory domain (Matsumoto et al., 2005; Sommer et al., 2005). This phosphorylation event activates CARD11 and, through an as yet unknown mechanism, activates the I $\kappa$ B kinases, which phosphorylate the I $\kappa$ B proteins, allowing them to be ubiquitinated and degraded. These events culminate in the unmasking of NF- $\kappa$ B's nuclear localization sequence, its translocation into the nucleus and the subsequent transcription of cytokines, pro-proliferative and anti-inflammatory genes.

CARD11 activity is regulated internally through ID-mediated autoinhibition. In the resting state, CARD11 is in a closed, inactive conformation mediated by intramolecular interactions between the ID and the N-terminal CARD, L1 and CC domains (McCully and Pomerantz, 2008). ID phosphorylation neutralizes the ID by triggering a conformational change in the protein. This exposes the N-terminal CARD, L1 and CC

domains and allows them to interact with several co-factors such as Bcl10, MALT1, TRAF6, the IKK complex and Caspase-8 (Bertin et al., 2001; Che et al., 2004; Gaide et al., 2001; McCully and Pomerantz, 2008; Shinohara et al., 2005; Shinohara et al., 2007; Wegener et al., 2006). In addition to the phosphorylation of S564 and S657 by PKC $\theta$ , it is also known that S567 phosphorylation by IKK $\beta$  and S577 phosphorylation by an unknown kinase play an important role in ID neutralization (Matsumoto et al., 2005; Shinohara et al., 2007; Sommer et al., 2005). Besides these modifications, HPK1 phosphorylation of S563 is necessary for downstream NF- $\kappa$ B activation (Brenner et al., 2009).

CARD11's ID is also modified after NF- $\kappa$ B activation to help downregulate signaling. Casein kinase 1  $\alpha$  (CK1 $\alpha$ ) has been shown to phosphorylate S620 and the serine to alanine mutation exhibits sustained NF- $\kappa$ B activation (Bidere et al., 2009). Similarly, the S649A mutation prevents phosphorylation by PKC $\beta$  and another novel kinase and results in enhanced NF-  $\kappa$ B signaling (Moreno-Garcia et al., 2009). Alternatively, phosphatase PP2A can inhibit CARD11 activity by removing the phosphate on S564 (Eitelhuber et al., 2011). Thus, it is increasingly evident that CARD11's ID is a central modulator of CARD11 activity and TCR or BCR signaling output.

The presence of CARD11 mutations in activated B-cell like diffuse large B-cell lymphoma (ABC-DLBCL) patients underlies its importance in humans. These mutations, found in about 10% of patients, have been characterized as gain-of-function mutations that lead to constitutive NF- $\kappa$ B activation and tumorigenesis (Compagno et al., 2009;

Davis et al., 2010; Lenz et al., 2008). Interestingly, these CARD11 hyperactive mutations were initially thought to be localized only in the CC domains; however, recent studies have uncovered lymphoma-associated CARD11 mutations in both the CARD domain and the LATCH domain, a portion of the linker between the CARD and CC with a high propensity for developing hyperactive mutants (Bu et al., 2012; Compagno et al., 2009; Dong et al., 2011; Lohr et al., 2012; Montesinos-Rongen et al., 2010). Mechanistic studies of several of these mutations indicated that they bypass ID-mediated autoinhibition by disrupting intramolecular binding (Chan et al., 2013; Lamason et al., 2010). Additionally, these CARD11 mutants spontaneously associated with Bcl10 specifically and promoted the nucleation with MALT1, but not other co-factors (Chan et al., 2013; Lamason et al., 2010).

From the CARD11 mutation studies, questions began to emerge about the subtleties of the ID mechanism of inhibition. With so many identified lymphoma-associated CARD11 mutations in the CARD, LATCH and CC domains, we did not understand why ID mutants had not been identified. It was also unclear how the ID regulated the association of Bcl10 and other co-factors. Here, we performed a systematic analysis of the ID to identify functional subdomains that regulate intramolecular binding, Bcl10 binding and signaling capacity for NF- $\kappa$ B activation. We describe a highly complex ID architecture of multiple functional elements that cooperatively modulate CARD11 activity.

**Chapter II: Functional Elements in CARD11's Inhibitory  
Domain Modulate NF- $\kappa$ B Activity**

## **CARD11's Inhibitory Domain contains multiple, redundant Repressive Elements**

In order to reveal the different functional regions of the ID, we first divided the ID into approximately six equal portions (Figure 2.2A). Utilizing downstream activation of an NF- $\kappa$ B responsive luciferase reporter, I $\kappa$ B2-IFN-Luc, in CARD11-deficient Jurkat T cells as a readout of CARD11 activity, we asked if inhibitory function could be restricted to any one of these regions. If this was the case, we would expect its deletion to mimic the hyperactivity seen in  $\Delta$ ID. As expected, wild-type murine CARD11 (WT) rescues the defect in  $\alpha$ CD3 and  $\alpha$ CD28-mediated NF- $\kappa$ B activation and  $\Delta$ 441-671 is constitutively active even in the absence of stimulation (Figure 2.2B, C). Our results also indicated that no single intradomain deletion affected ID function in the basal state, implying that multiple, redundant regions of the ID were capable of exerting some repressive function (Figure 2.2B, C). Moreover, residues 530-616 were necessary for reversing ID inhibition. Of note, the deletion of S657, a previously identified PKC $\theta$  phosphorylation site, had no effect on ID neutralization (Figure 2.2B, C).

We then went on to map the different regions of the ID having some repressive function, which we termed repressive elements (REs). They are depicted in Figure 2.1. To identify these elements, we took a minimalist approach. In the context of  $\Delta$ ID, we sequentially added intradomain regions onto the N-terminus of the ID and assessed which regions were capable of repressing the activity of  $\Delta$ ID (Figure 2.3A). The first 90 amino acids of the ID, which we named RE1, conferred 4.8 fold repression over  $\Delta$ ID (Figure 2.3B, C). The boundaries of RE1 were further narrowed down to the first 53 amino acids



of the ID (Figure 2.4). CARD11 residues 530-610 further repressed CARD11 activity four fold, hinting at the presence of another RE among these residues (Figure 2.3B, C).

To circumvent the redundancy of the REs, we reversed our sequential addition to add C-terminal ID intradomain regions onto  $\Delta$ ID to assess CARD11 inhibition (Figure 2.5A). Surprisingly, the last 17 residues of the ID displayed constitutive hyperactivity more than fivefold greater than that seen with  $\Delta$ ID (Figure 2.5B, C). This hyperactivity was indicative of a novel activating element (AE). Our analysis also revealed a clear RE, designated RE4, that repressed the hyperactivity of AE almost 100 fold and was 16 fold repressed compared to  $\Delta$ ID (Figure 2.5B, C). This RE was restricted to CARD11 residues 617-641 (Figure 2.6).

The redundancies of REs made it difficult to characterize the possible RE between CARD11 residues 530-610. Thus, we sought to mutate RE1 and RE4 and reevaluate repressive function in our addition analysis. Because CARD11 residues 484-493 possessed 38 fold repressive potential in RE1, we specifically targeted these residues for mutagenesis (Figure 2.4 and Figure 2.7A). By contrast, three or four residue mutations covering all 25 amino acids of RE4 were examined (Figure 2.8A). Both RE1 mutations tested diminished the repressive abilities of RE1 by at least two fold (Figure 2.7B, C). While some RE4 mutants had a modest effect on CARD11 activation, three of the eight mutants completely abolished repression (Figure 2.8B, C). M1 and M9 were then chosen for further studies of RE1 and RE4, respectively.

With RE1 mutated, we repeated our C-terminal ID addition analysis and found that amino acids 568-610 added about 2.5 fold repression (Figure 2.9A, B, C). The

evidence of a repressive element in these residues was even more compelling in the RE4 mutant context where it conferred over 300 fold inhibition (Figure 2.9A, D, E). Notably, we observed that residues 536-573 had substantial activating capacity. This activity was more pronounced in the RE4 N-terminal ID addition analysis, where there was a 30 fold increase in activation (Figure 2.9D, E). This data also suggests the full activity of this element may extend beyond residue 536.

When mapping the boundaries of the newly uncovered repressive element, we actually detected two, non-overlapping REs (Figure 2.10A). The CARD11 residues 574-599, labeled RE2, had over 100 fold repressive capacity (Figure 2.10B, C). This RE was further constricted to residues 586-599 (data not shown). The other identified RE, RE3, spanned residues 600-610 and was similar to RE2 in its repressive potency (Figure 2.10B, C).

Close examination of the sequence of RE2 and RE3 indicated strong sequence homology between the two. Both possessed a hydrophobic residue, followed by three acidic residues and an asparagine (Figure 2.10A). We hypothesized that RE2 and RE3 function was dependent on this homologous sequence. To test this possibility, we mutated the three acidic residues to basic residues and asked if this abrogated RE2 or RE3 function (Figure 2.10A). We discovered that mutating the acidic residues of RE2 or RE3 alone was not sufficient to bestow hyperactivity, but that mutating RE2 and RE3 consecutively achieved hyperactivity at least 75% of that seen in the absence of the two REs (Figure 2.10B, C). Thus, we concluded that RE2 and RE3 function required this homologous region.

Because we wanted to carry out an exhaustive analysis of the ID, we probed for extra obscured repressive elements by repeating our N-terminal ID addition assay in the presence of simultaneously mutated RE2, RE3 and RE4. This analysis confirmed no other repressive elements in the ID (data not shown). Taken together, we discovered four independent and redundant repressive elements that could inhibit CARD11 activity.

### **CARD11's Inhibitory Domain contains two independent Activating Elements**

Since our initial mapping of RE2 and RE3 hinted at the existence of a second activating element, we aimed to isolate this sequence and confirm its activating potential (Figure 2.9). Importantly, we wanted to see if the activating element was separable from RE2. To this end, we isolated residues 536-585 and ascertained what effect they had on CARD11  $\Delta$ ID activity. Indeed, these residues were sufficient to cause CARD11 hyperactivity (data not shown). Then, we wanted to determine the minimal region of this activating element and found that residues 547-585 formed a *de facto* activating element AE1 (Figure 2.11B, C). These residues possessed 6.5 fold higher activity than  $\Delta$ ID and over 600 fold higher activity compared to CARD11 WT (Figure 2.11B, C). In addition, we saw that AE1 and AE2 in tandem was slightly more active than either AE alone, suggesting some redundancy in activating element function (Figure 2.11B, C). Overall, the activity of both AEs together, which was about 800 fold higher than WT and about eight fold higher than  $\Delta$ ID, represents the highest level of potential CARD11 activity achieved thus far.

## **CARD11's Inhibitory Domain contains a single Inducibility Element**

Although it is known that several residues of CARD11 are known to be modified upon antigen receptor signaling, we wanted to identify which of these residues was necessary for inducing CARD11 activity after stimulation. In order to do this, we re-examined our intradomain deletions for regions that, when deleted, reduced stimulated CARD11 activity. As expected, deletion of amino acids 530-573, which deletes known PKC $\theta$  phosphorylation site S564 or deletion of 568-616, which deletes known IKK $\beta$  phosphorylation site S567 resulted in a loss of activity after  $\alpha$ CD3 and  $\alpha$ CD28 stimulation (Matsumoto et al., 2005; Shinohara et al., 2007; Sommer et al., 2005) (Figure 2.2). Similarly, deletion of S577, a known *in vivo* phosphorylation site, attenuated CARD11 induction post stimulation (Matsumoto et al., 2005) (Figure 2.2). Surprisingly, deletion of S657 had no effect on inducing CARD11 activity even though it was previously characterized as a PKC $\theta$  substrate (Matsumoto et al., 2005; Sommer et al., 2005) (Figure 2.2). This analysis led us to conclude that CARD's ID neutralization occurs through a contiguous inducibility element (IE) that spanned residues 530-616.

To further map this IE, we sequentially deleted the ID residues 530-616 from the N-terminus and C-terminus and assessed them for their induction of CARD11 activity with stimulation (Figure 2.12A). Our data suggested that the induction of CARD11 requires residues 561-585 (Figure 2.12B, C). Importantly, these residues were sufficient to reverse the inhibition of all four repressive elements as seen in  $\Delta$ 530-560  $\Delta$ 611-616 (Figure 2.11B, C).

## **CARD11's Repressive Elements require multiple mutations to abolish RE function**

With so many repressive elements embedded within the ID, we wanted to better understand how they functioned together with both activating elements and the inducibility element. To do this, we first mutated all four repressive elements in the full-length CARD11 context (Figure 2.13A). We expected that destroying all RE function in the ID would bypass the need of the inducibility element and result in CARD11 basal activation equivalent to that of having two activating elements. Instead, we saw that mutating all four REs simultaneously only resulted in activity similar to that of deletion of the entire ID (Figure 2.13B, C).

Because our mutational analysis of RE4 was performed only in the context of AE2, we hypothesized that the presence of other ID sequences may necessitate the need of supplementary mutation in RE4 to completely diminish its repressive function in the full-length context. Our initiation RE4 mutational analysis suggested multiple possible secondary mutations from which to choose (Figure 2.8B, C). M5 was chosen as the second site RE4 mutation because it had a substantial effect on RE4 repression without being adjacent to M9, insinuating that this mutation might function by a different mechanism from M9 (Figure 2.8B, C). The quadruple RE mutant construct with two RE4 mutations did, in fact, increase CARD11 activity fivefold, making it as active as AE2 (Figure 2.13B, C). This result indicated that this version of the quadruple RE mutant still did not achieve levels of activity similar to AE1+AE2.

Since our RE1 mutant analysis simply tested for the ability to destroy intrinsic repression, it did not assay for repression of other ID elements. The limitation of that analysis led us to test if a second RE1 mutation could boost quadruple RE mutant activity. Hence, we tested two additional RE1 mutants M13 and M14 for their ability to increase quadruple RE mutant activity (Figure 2.13B, C). We observed that two mutations in RE1, one mutation in RE2, one mutation in RE3 and two mutations in RE4 for a total of six mutations of 28 total residues in the ID resulted in about 800 fold increase in activity compared to WT and about 8 fold higher when compared to  $\Delta$ ID (Figure 2.13B). Hence, this version of the quadruple RE mutant reached levels of activity similar to that of both activating elements together. From hereon forward, we will refer to this construct as the quadruple RE mutant.

### **CARD11's Repressive Elements cooperate to repress downstream signaling to NF- $\kappa$ B**

Because of the discrepancy between the effects of RE1 and RE4 mutations in a minimal context and the full-length context, we sought to characterize what effects all the RE mutations would exert on CARD11 activity in the full-length context. To do this, we designed CARD11 ID single, double and triple RE mutant combination constructs (Figure 2.14A). The activities of these CARD11 variants would attest to how the REs function in combination with AE1 and AE2. Not surprisingly, we found that mutating each RE alone had little to no effect on CARD11 activity, confirming the redundancy of the four REs (Figure 2.14B, C and Table 2.4). The mutant RE4 increased basal activity

about three fold, the most of all the single RE mutants (Figure 2.14B, C). This finding suggests that RE4 may be the strongest repressor. We also asserted that no RE affected CARD11's inducibility (Figure 2.14B).

Similar to the single RE mutants, most double RE mutants were relatively repressed. All the double mutants increase CARD11 activity at least four fold over WT; however, the RE1 and RE4 double mutant increased downstream NF- $\kappa$ B activity almost 70 fold (Figure 2.14D, E and Table 2.4). This result indicated that two REs are sufficient to mostly inhibit CARD11 activity and that RE1 and RE4 are the two most potent REs.

Triple RE mutants were viewed from the perspective of how much a single, intact RE could contribute to overall CARD11 inhibition. Unexpectedly, all triple RE mutants were at least as active as  $\Delta$ ID (Figure 2.14F, G and Table 2.4). In the full-length context, a single RE was insufficient to inhibit CARD11 activity. This analysis also confirmed that RE4 was the most potent RE, followed by RE1. Altogether, these results imply that the REs work together to repress CARD11.

### **Bcl10 association is regulated by multiple Repressive Elements**

After determining the relative contributions of each RE to regulate CARD11 activity, we asked how each RE regulated the association of co-factors. Bcl10 was of particular interest because its association was sufficient to generate hyperactivity in several previously described lymphoma-associated CARD11 variants (Chan et al., 2013; Lamason et al., 2010). Therefore, we specifically examined how each RE affected Bcl10 association. Although the quadruple RE mutant was noticeably more active than  $\Delta$ ID, its

level of Bcl10 association was similar to that of  $\Delta$ ID (Figure 2.15). Furthermore, no single RE mutation significantly upregulated Bcl10 association (Figure 2.15A). In contrast, all double RE mutants having RE1 mutated showed appreciable levels of Bcl10 association compared to WT CARD11 (Figure 2.15B). Likewise, having RE1 mutated with any two other REs bound to Bcl10 as well as the quadruple RE mutant and  $\Delta$ ID (Figure 2.15C). Thus, RE1 was the major contributor to prevent Bcl10 association. Nevertheless, the other REs cooperatively regulated Bcl10 binding (Figure 2.15B, C). Curiously, the degree of Bcl10 association did not correlate with the level of CARD11 activity.

### **CARD11's Repressive Elements synergize to control intramolecular binding**

Another possible mechanism by which the REs may function is by modulating intramolecular binding. To determine if any RE functioned by regulating binding to other regions of CARD11, we first generated an N-terminal Flag-GST-tagged ID. If an RE mutant disrupted intramolecular binding sites, it would allow a full-length WT ID expressed *in trans* to bind the inherent RE binding targets. As predicted, mutating all four REs markedly increased binding to WT ID *in trans* (Figure 2.16). A single RE did not act as the only determinant of conformational state because no single RE mutant was able to bind the ID *in trans* at appreciable levels (Figure 2.16A). Unexpectedly, mutating two RE mutants was sufficient to detect disruptions in intramolecular contacts (Figure 2.16B). All triple RE mutants also appeared to be in the open conformation (Figure 2.16C). Because



there was a discernible difference in ID binding for RE combination mutants having a WT or mutant RE1, it appeared that RE1 was the dominant player in regulating CARD11 conformation (Figure 2.16). Our data also demonstrates the synergistic effect of the REs on altering intramolecular binding.

### **Repressive Elements bind differential CARD11 intramolecular targets**

In order to ascertain the binding site for each RE, we first assayed whether a single RE tetramer could mediate binding to  $\Delta$ ID, which is constitutively in the open conformation. We found that all four RE tetramers were sufficient to bind  $\Delta$ ID to some extent (Figure 2.17). The extremely weak binding of RE4 led us to believe its binding target may be within the ID itself. In order to reveal novel intramolecular RE targets within the ID, we investigated whether any RE could bind its corresponding full-length single RE mutant. Because the single RE mutant lacked the ability to bind its respective intramolecular target, these targets would be free to bind the RE tetramer *in trans*. We saw that RE4 tetramer was unable to bind the single RE4 CARD11 mutant, suggesting that it does not bind within the ID and it is a weak contributor to maintaining intramolecular contacts. The lack of binding of the other REs to their respective single RE CARD11 mutants in this assay hinted at redundant RE binding to each CARD11 target (Figure 2.17).

Though all our data so far suggested that all four REs contributed to intramolecular binding, we hypothesized that each RE would bind differentially and that this distinction in target binding resulted in the difference in repressive potency. To

identify the CARD11 domain targets of each RE, we tested binding of the three strongest REs to bind a panel of CARD11 double-deletion variants where each domain of CARD11 was deleted simultaneously with the ID deletion. Deletion of the coiled-coiled domain (CC) and the guanylate kinase domain (GUK) diminished binding of RE1 tetramers (Figure 2.18A). Interestingly, this analysis revealed the linker between PDZ and SH3 domains (L3) and SH3 domains were inhibitors of RE1 tetramer binding (Figure 2.18A). RE2 tetramer binding to  $\Delta$ ID required the CARD domain, the linker between the CARD domain and the CC domain (L1) and, to a lesser extent, the CC domain (Figure 2.18B). The RE3 tetramers had a unique domain requirement for binding to  $\Delta$ ID compared to RE1 and RE2 as it only required the CARD domain and the CC domains (Figure 2.18C). Thus, each RE has a distinct target binding profile.

### **Lymphoma-associated, gain-of-function CARD11 mutations disrupt binding of at least two Repressive Elements**

Based on the partially redundant binding targets of the REs, we speculated that lymphoma-associated single point mutations in CARD11's CARD, LATCH or CC domains disrupted binding to multiple REs allowing them to bypass ID neutralization and lead to hyperactive CARD11. Because all of the gain-of-function CARD11 mutants were at least as active as the most repressed double RE mutants (Chan et al., 2013; Lamason et al., 2010), we expected that the lymphoma-associated mutants C49Y, F97Y, G123D, F130I and L232LI would reverse the effects of at least two REs. Interestingly, RE1 tetramer binding was abated by mutations in all three domains even though RE1 tetramer

binding did not require the LATCH domain (Figure 2.18A, Figure 2.19A). As anticipated, both CARD mutants C49Y and F97Y and both LATCH mutants G123D and F130I, but not the CC mutant L232LI decreased RE2 tetramer binding (Figure 2.18B, Figure 2.19B). RE3 tetramer binding was compromised by mutations in the CARD, LATCH and CC domains despite only requiring the CARD and CC domains for binding (Figure 2.18C, Figure 2.19C). Indeed, all five oncogenic mutants tested at least partially disrupted binding to two REs with four of the five mutants obstructing binding to all three REs (Figure 2.19).

## **Experimental Procedures**

### **Cell lines and expression constructs**

HEK 293T and human Jurkat T cell lines were cultured as previously described (McCully and Pomerantz, 2008).

pcMycCARD11 WT,  $\Delta$ ID,  $\Delta$ ID double deletions,  $\Delta$ ID C49Y,  $\Delta$ ID F97Y,  $\Delta$ ID G123D,  $\Delta$ ID F130I and  $\Delta$ ID L231LI were described previously (Chan et al., 2013; Lamason et al., 2010; McCully and Pomerantz, 2008). Various CARD11 deletion constructs were cloned by standard molecular biology techniques and sequence verified. All ID deletion constructs along with their corresponding amino acid linkers are listed in Table 2.1. Mutations were introduced into CARD11 by PCR or by QuikChange Site-Directed Mutagenesis (Stratagene) using the primers listed in Table 2.2 and are described in Table 2.3. Flag-tagged Bcl10 was described previously.

To generate pEBB-Flag-GST-ID, a DNA fragment of CARD11 corresponding to CARD11 amino acids 441-671 was cloned into pEBB in frame with an N-terminal Flag tag and GST derived from pEBG (McCully and Pomerantz, 2008). pEBB-Flag-GST is a variant of the above construct that encodes a stop codon after GST. To generate Flag-GST-RE multimers, the full-length ID in pEBB-Flag-GST-ID was replaced with four copies of the DNA encoding RE1, RE2, RE3 or RE4 corresponding to CARD11 residues 441-493, 586-599, 600-610 or 617-641, respectively.

### **HEK 293T protein expression assay**

Cells were plated at  $5 \times 10^5$  cells in 2ml media onto each well of a 6-well plate 24 hours prior to transfection. Cells were transfected with 200ng pCSK-LacZ, 1500ng Ig $\kappa$ <sub>2</sub>-IFN-Luc and up to 1300ng of expression construct, totaling 3 $\mu$ g DNA. In each experiment, samples were supplemented with empty pcDNA3 vector to keep the total amount of DNA per transfection constant. The media was changed 22-25 hours post transfection and harvested 40-42 hours post transfection. Cells were lysed in 500 $\mu$ l lysis buffer (Promega) on ice. Cells were scrapped from the plate and incubated with lysis buffer on ice at least 10 minutes before cell debris was cleared by centrifugation 17,970 x g for 5 min at 4°C. Three microliters of lysate was used to measure  $\beta$ -galactosidase activity in a chemiluminescent  $\beta$ -Gal reporter gene assay (Roche) according to the manufacturer's instructions. Chemiluminescence was measured by a luminometer (Perkin Elmer TR717 or Berthold Technologies TriStar LB 941 Multimode Microplate Reader) integrating for 10s after a 2-s delay. B-galactosidase activity was used to normalize

lysates for transfection efficiency and recovery. Normalized lysates were resolved on an 8% SDS-PAGE gel, transferred to polyvinylidene difluoride membrane and analyzed by Western blot with anti-myc (sc-40; Santa Cruz) antibodies for relative expression.

### **Determination of CARD11 activity in Jurkat T cells**

The production of stable CARD11 knockdown Jurkat T cells was performed as previously described, except that polybrene was excluded from the infection (McCully and Pomerantz, 2008). MISSION Non-Target shRNA Control Vector (Sigma SHC002; sense sequence: 5' CAACAAGATGAAGAGCACCAA 3'; loop sequence: 5' CTCGAG 3') was used as a control. CARD11 knockdown Jurkats were transiently transfected with Ig $\kappa$ <sub>2</sub>-IFN-Luc, pCSK-LacZ and pcCARD11 variants, stimulated and harvested as described previously (McCully and Pomerantz, 2008). All results shown are the average ( $\pm$ std. dev.) of triplicate samples from a single experiment, representative of two or three that were performed.

### **HEK 293T Immunoprecipitations**

Immunoprecipitations were performed as previously described, except for the following (Chan et al., 2013). At 40-42 hours post transfection, cells were harvested in 500 $\mu$ l immunoprecipitation lysis buffer (IPLB), incubated on ice 10 minutes, scrapped off and centrifuged at 17,970 x g for 5 minutes at 4°C. Eleven microliters of lysate was reserved for Western blot analysis and 440  $\mu$ l lysate used for immunoprecipitation with anti-Flag antibody. Input and IP elutions were resolved by immunoblot using anti-myc

(sc-40; Santa Cruz) and anti-FLAG (M2; Eastman Kodak IB13026 or Sigma F1804) antibodies as described previously (Chan et al., 2013). Results shown are the representative of two or three assays that were performed.

### **HEK 293T Glutathione Sepharose Pull-down**

Cells were plated at  $5 \times 10^5$  cells per well in 6-well plates 24 hours prior to transfection. Cells were transfected using the calcium phosphate method with up to 1400ng Flag-GST variants and up to 750ng CARD11 variants. In each experiment, additional pcDNA3 and pEBB vectors were transfected such that each well was transfected with equal amounts of pcDNA3 vector and pEBB vector and totaled  $2 \mu\text{g}$  DNA. Media was changed 22-25 hours post transfection and harvested as described previously, except as follows (McCully and Pomerantz, 2008). Cells were lysed in 500 $\mu\text{l}$  IP Lysis Buffer, precleared twice for 30 minutes with 10 $\mu\text{l}$  Protein G Sepharose Fast Flow (GE Healthcare) with 4°C rotation. From the precleared lysate 2% or 3% of lysate was reserved for input. The remaining lysate was incubated with 10 $\mu\text{l}$  bed volume of glutathione-Sepharose (GE Healthcare) for 3 hours at 4°C with rotation. Samples were washed and analyzed as described previously (McCully and Pomerantz, 2008). Western blotting was completed using anti-myc (Santa Cruz, sc-40) and anti-GST (Santa Cruz, sc-459) antibodies. Results shown are the representative of two or three assays that were performed.

## Tables

**Table 2.1: CARD11 deletion and mutant constructs.**

CARD11 Constructs	Alternative Names	Linker	Mutation	Amino Acid Mutations
Δ441-671	ΔID	RS	—	
Δ441-671	Δ5'-3'	TG	—	
Δ441-488	Δ5'-A	TGRD	—	
Δ483-535	ΔA-B	RKTGKR	—	
Δ530-573	ΔB-C	DNTGDR	—	
Δ568-616	ΔC-D	RRTGRD	—	
Δ611-654	ΔD-E	DKTGKD	—	
Δ649-671	ΔE-3'	RDTG	—	
Δ483-671	ΔA-3'	RKTG	—	
Δ530-671	ΔB-3'	DNTG	—	
Δ568-671	ΔC-3'	RRTG	—	
Δ611-671	ΔD-3'	DKTG	—	
Δ504-671	ΔA2-3'	TG	—	
Δ494-671	ΔA1-3'	TG	—	
Δ441-459	Δ5'-5'1	TG/	—	
Δ494-671	ΔA1-3'	TG	—	
Δ441-469	Δ5'-5'2	TG/	—	
Δ494-671	ΔA1-3'	TG	—	
Δ441-478	Δ5'-5'3	TG/	—	
Δ494-671	ΔA1-3'	TG	—	
Δ441-486	Δ5'-A	TG/	—	
Δ494-671	ΔA1-3'	TG	—	
Δ494-671	ΔA1-3'+ mut A	TG	M1	483 SPEDSK 488: RKTGRD
Δ494-671	ΔA1-3'+ mut YFLPY	TG	M2	489 YFLPY 493: ADRKA
Δ441-535	Δ5'-B	TGKR	—	
Δ441-573	Δ5'-C	TGDR	—	
Δ441-616	Δ5'-D	TGRD	—	
Δ441-654	Δ5'-E	TGKD	—	

CARD11 Constructs	Alternative Names	Linker	Mutation	Amino Acid Mutations
Δ441-616 Δ624-654	Δ5'D ΔD1-E	TGRD/ TGKD	—	
Δ441-616 Δ633-654	Δ5'D ΔD2-E	TGRD/ TGKD	—	
Δ441-616 Δ642-654	Δ5'D ΔD3-E	TGRD/ TGKD	—	
Δ441-623 Δ649-654	Δ5'-D1 +mut E	TG/ RDTGKD	—	
Δ441-632 Δ649-654	Δ5'-D2 +mut E	TG/ RDTGKD	—	
Δ441-641 Δ649-654	Δ5'-D3 +mut E	TG/ RDTGKD	—	
Δ441-616	Δ5'-D+ mut GPPS	TGRD	M3	617 GPPS 620: WQHK
Δ441-616	Δ5'-D+ mut IHS	TGRD	M4	621 IHS 623: RFR
Δ441-616	Δ5'-D+ mut SSS	TGRD	M5	624 SSS 626: RRR
Δ441-616	Δ5'-D+ mut SHQ	TGRD	M6	627 SHQ 629: RFA
Δ441-616	Δ5'-D+ mut SEG	TGRD	M7	630 SEG 632: RRW
Δ441-616	Δ5'-D+ mut LDA	TGRD	M8	633 LDA 635: RKR
Δ441-616	Δ5'-D+ mut YDL	TGRD	M9	636 YDL 638: AKR
Δ441-616	Δ5'-D+ mut EQV	TGRD	M10	639 EQV 641: RAK
Δ530-671	ΔB-3'+ mut A	DNTG	M1	483 SPEDSK 488 : RKTGRD
Δ568-671	ΔC-3'+ mut A	RRTG	M1	483 SPEDSK 488 : RKTGRD
Δ611-671	ΔD-3'+ mut A	DKTG	M1	483 SPEDSK 488 : RKTGRD



CARD11 Constructs	Alternative Names	Linker	Mutation	Amino Acid Mutations
Δ441-573 Δ611-616	Δ5'C+ mut D+ mut YDL	TGDR/ DKTGRD	M9	636 YDL 638: AKR
Δ441-535 Δ611-616	Δ5'B+ mut D+ mut YDL	TGKR/ DKTGRD	M9	636 YDL 638: AKR
Δ441-488 Δ611-616	Δ5'A+ mut D+ mut YDL	TGRD/ DKTGRD	M9	636 YDL 638: AKR
Δ441-573	Δ5'-C+ mut YDL	TGDR	M9	636 YDL 638: AKR
Δ441-573 Δ600-616	Δ5'-C ΔC4-D+ mut YDL	TGDR/ AGRD	M9	636 YDL 638: AKR
Δ441-599 Δ611-616	Δ5'-C4+ mut D+ mut YDL	TG/ DKTGRD	M9	636 YDL 638: AKR
Δ441-573	Δ5'C+ mut EED+ mut YDL	TGDR	M9, M11	636 YDL 638: AKR 593 EED 595: RRR
Δ441-573	Δ5'C+ mut DDE+ mut YDL	TGDR	M9, M12	636 YDL 638: AKR 607 DDE 609: RRR
Δ441-573	Δ5'C+ mut EED+ mut DDE+ mut YDL	TGDR	M9, M11, M12	636 YDL 638: AKR 593 EED 595: RRR 607 DDE 609: RRR
Δ441-546 Δ586-671	Δ5'B2 ΔC2-3'	TG/ AG	—	
Δ441-546 Δ586-654	Δ5'B2 ΔC2-E	TG/ AGKD	—	
Δ530-535 Δ611-616	mutB+D	DNTGKR/ DKTGRD	—	
Δ530-560 Δ611-616	ΔB-B4 +mutD	DNTG/ DKTGRD	—	

<b>CARD11 Constructs</b>	<b>Alternative Names</b>	<b>Linker</b>	<b>Mutation</b>	<b>Amino Acid Mutations</b>
$\Delta$ 530-567 $\Delta$ 611-616	$\Delta$ B-B5 +mutD	DNTG/ DKTGRD	—	
$\Delta$ 530-535 $\Delta$ 586-616	mutB+ $\Delta$ C2-D	DNTGKR/ AGRD	—	
$\Delta$ 530-535 $\Delta$ 579-616	mutB+ $\Delta$ C1-D	DNTGKR/ AGRD	—	
$\Delta$ 530-560 $\Delta$ 586-616	$\Delta$ B-B4 $\Delta$ C2-D	DNTG/ AGRD	—	

Table 2.2: CARD11 mutant primers and oligos.

CARD11 Mutation	Alternative Name	Strategy <sup>1</sup>	Oligo	Oligo Sequence	Cloning Sites
M13	mut Q	oligo	5' oligo 1	GAGTCTGCCTAGACACCTTCCAGCCACCATCATCTCA	PshAI-AgeI
			3' oligo 1	TCACTGAGATCATGGTGGCTGGAAGGTGCTAGGCAGACTC	
			5' oligo 2	GTGACCTAATGAAGCAATGGGCCGAGTTC	
			3' oligo 2	CATTGAGCTCGGCCCAATTGCTTCATGTAGG	
			5' oligo 3	AATGGCCAGGAAGCTGATGATTCTTCAACCTCAGAAGAGCGGAAGA	
			3' oligo 3	CCGGTCTTCGGCTCTTCTGAGGTGAAGAAATCATCAGCTTCCCTGGC	
M14	mut N	oligo	5' oligo 1	GAGTCTGCCTAGACACCTTCCAGCCACCATCATCTCA	PshAI-AgeI
			3' oligo 1	TCTGTGAGATGATGGTGGCTGGAAGGTGCTAGGCAGACTC	
			5' oligo 2	CAGAACCTTGGAGACACCAGCCCCAGGACC	
			3' oligo 2	TAGTGGTCTGGGGTGGTGTCTCCAAGGT	
			5' oligo 3	ACTATCGCGCGAAATGAAGAGTTTTCAACCTCAGAAGAGCGGAAGA	
			3' oligo 3	CCGGTCTTCGGCTCTTCTGAGTTGAAAACCTTCTTCATTCGGCGGA	
M1	mut A	2-step PCR	5' oligo	CGGAAGACCGGTAGGGACTACTTCTGCCTTACCACCACCCCGG	PshAI-ApaI
			3' oligo	GTCCCTACCGGTCTTCGGCTCTTCTGAGTTGAAGATCATCAGCTTCC	
M2	mut YFLPY	PCR	3' oligo	CATTACCGGTTCGCTTCCTATCGGCCCTTGGCTGTCTTCGGGAGACTC	PshAI-AgeI
M11	mut EED	QC	5' oligo	CGCCACACCGGAGCACGGTGCCTCGCCGAAACGATAGCTGTGGGTTTG	PshAI-PmlI
			3' oligo	CAAAACCCACAGCTATCGTTTTCGGCGAAGCACCGTGTCTCGGTGTGGG	
M12	mut DDE	QC	5' oligo	GGTTTGTATGCCTTAGACCTTCGGCGCCGAAATCAGAACGTTATTCC	PshAI-PmlI
			3' oligo	GGAAATAACGTTGGTATTCGGGCGGAAGGTCTAAGGCATCAAAACCC	
M3	mut GPPS	PCR	5' oligo	GACCGTCCGGACTGGCAGCATAAATCCACTCCTCCTCTTCACAC	AgeI-PmlI
M4	mut IHS	QC	5' oligo	GGGACGGACCTCCCTCCCGCTTTCCTCCTCTTCACACCAG	AgeI-PmlI
			3' oligo	CTGGTGTGAAGAGGAGGACGAAACCGGGAGGAGTCCGTCCC	
M5	mut SSS	QC	5' oligo	CTCCCTCCATCCACTCCCGCCCGGCTCACACCAGTCAAGG	AgeI-PmlI
			3' oligo	CCTCTGACTGGTGTGAGCCGGCGGGGAGTGGATGGAGGGAG	
M6	mut SHQ	2-step PCR	5' oligo	CGCTTGCATCAGAGGACTGGATGCCCTACGACCTGGAGC	AgeI-PmlI
			3' oligo	TCCAGTCCCTCTGATGCAAAAGCCAGGAGGAGTGGATGGAGGGAG	
M7	mut SEG	2-step PCR	5' oligo	CGAAGATGGTGGATGCCCTACGACCTGGACAGGTCAACC	AgeI-PmlI
			3' oligo	CGTAGGCATCCAGCCATCTTCGCTGGTGTGAAGAGGAGGAGTGGAT	

CARD11 Mutation	Alternative Name	Strategy <sup>1</sup>	Oligo	Oligo Sequence	Cloning Sites
M8	mut LDA	2-step PCR	5' oligo	CGGAAAGCGCTACGACCTGGAGCAGGTCAACCTCATGTTCACGAAAGT	AgeI-PmlI
			3' oligo	CCAGGTGCTAGCGCTTCCCGTCCCTCTGACTGGTGTGAAGAGGAGGAGG	
M9	mut YDL	2-step PCR	5' oligo	GCCAAAGCGGAGCAGGTCAACCTCATGTTCGAAAGTCTCTTTGGA	AgeI-PmlI
			3' oligo	GTTGACCTGCTCCCGCTTGGCGGCATCCAGTCCCTCTGACTGGTGTGA	
M10	mut EQV	2-step PCR	5' oligo	CGCGCCAAAGAACCTCATGTTCGAAAGTCTCTTTGAAAGGCCCTTCC	AgeI-PmlI
			3' oligo	CGTAAACATGAGGTTCTTGGCGGCAGGTCGTAGGCATCCAGTCCCTCTG	

<sup>1</sup> Strategy options are as follows: oligo = mutation introduced by synthetic oligonucleotides, 2-step PCR = fusion PCR with mutant introduced into primers, PCR = mutation introduced into sequence through single primer in one PCR reaction, QC = mutation introduced by QuikChange reaction and backcloning

**Table 2.3: CARD11 full-length mutant constructs.**

CARD11 Mutant	Alternate Name	Alternate Name2	Amino Acid Mutations
M1		mut A+	483 SPEDSK 488 : RKTGRD
M11		mut EED+	593 EED 595: RRR
M12		mut DDE+	607 DDE 609: RRR
M9		mut YDL	636 YDL 638: AKR
M1		mut A+	483 SPEDSK 488 : RKTGRD
M11		mut EED+	593 EED 595: RRR
M12		mut DDE+	607 DDE 609: RRR
M5		mut SSS+	624 SSS 626: RRR
M9		mut YDL	636 YDL 638: AKR
M13		mut Q+	460 QNLGDTSPRT 469: VTYMKQWAEI
M1		mut A+	483 SPEDSK 488 : RKTGRD
M11		mut EED+	593 EED 595: RRR
M12		mut DDE+	607 DDE 609: RRR
M5		mut SSS+	624 SSS 626: RRR
M9		mut YDL	636 YDL 638: AKR
M14		mut N+	470 NGQEADDS 477: TIARMKKF
M1		mut A+	483 SPEDSK 488 : RKTGRD
M11		mut EED+	593 EED 595: RRR
M12		mut DDE+	607 DDE 609: RRR
M5		mut SSS+	624 SSS 626: RRR
M9		mut YDL	636 YDL 638: AKR
M13	re1	mut Q+	460 QNLGDTSPRT 469: VTYMKQWAEI
M1	RE2	mut A	483 SPEDSK 488 : RKTGRD
	RE3		
	RE4		
M11	RE1	mut EED	593 EED 595: RRR
	re2		
	RE3		
	RE4		
M12	RE1	mut DDE	607 DDE 609: RRR
	RE2		
	re3		
	RE4		

CARD11 Mutant	Alternate Name	Alternate Name2	Amino Acid Mutations
M5	RE1	mut SSS+	624 SSS 626: RRR
M9	RE2	mut YDL	636 YDL 638: AKR
	RE3		
	re4		
M13	re1	mut Q+	460 QNLGDTSPRT 469: VTYMKQWAE
M1	re2	mut A+	483 SPEDSK 488 : RKTGRD
M11	RE3	mut EED	593 EED 595: RRR
	RE4		
M13	re1	mut Q+	460 QNLGDTSPRT 469: VTYMKQWAE
M1	RE2	mut A+	483 SPEDSK 488 : RKTGRD
M12	re3	mut DDE	607 DDE 609: RRR
	RE4		
M13	re1	mut Q+	460 QNLGDTSPRT 469: VTYMKQWAE
M1	RE2	mut A+	483 SPEDSK 488 : RKTGRD
M5	RE3	mut SSS+	607 DDE 609: RRR
M9	re4	mut YDL	636 YDL 638: AKR
M11	RE1	mut EED+	593 EED 595: RRR
M12	re2	mut DDE	607 DDE 609: RRR
	re3		
	RE4		
M11	RE1	mut EED+	593 EED 595: RRR
M5	re2	mut SSS+	624 SSS 626: RRR
M9	RE3	mut YDL	636 YDL 638: AKR
	re4		
M12	RE1	mut DDE+	607 DDE 609: RRR
M5	RE2	mut SSS+	624 SSS 626: RRR
M9	re3	mut YDL	636 YDL 638: AKR
	re4		
M13	re1	mut Q+	460 QNLGDTSPRT 469: VTYMKQWAE
M1	re2	mut A+	483 SPEDSK 488 : RKTGRD
M11	re3	mut EED+	593 EED 595: RRR
M12	RE4	mut DDE	607 DDE 609: RRR

CARD11 Mutant	Alternate Name	Alternate Name2	Amino Acid Mutations
M13	re1	mut Q+	460 QNLGDTSPRT 469: VTYMKQWAEL
M1	re2	mut A+	483 SPEDSK 488 : RKTGRD
M11	RE3	mut EED+	593 EED 595: RRR
M5	re4	mut SSS+	624 SSS 626: RRR
M9		mut YDL	636 YDL 638: AKR
M13	re1	mut Q+	460 QNLGDTSPRT 469: VTYMKQWAEL
M1	RE2	mut A+	483 SPEDSK 488 : RKTGRD
M12	re3	mut DDE+	607 DDE 609: RRR
M5	re4	mut SSS+	624 SSS 626: RRR
M9		mut YDL	636 YDL 638: AKR
M11	RE1	mut EED+	593 EED 595: RRR
M12	re2	mut DDE+	607 DDE 609: RRR
M5	re3	mut SSS+	624 SSS 626: RRR
M9	re4	mut YDL	636 YDL 638: AKR

**Table 2.4: Relative activities of CARD11 full-length RE mutants.**

<b>CARD11 Variant</b>	<b>Relative Activity<sup>1</sup></b>	<b>Fold Repressed<sup>2</sup></b>
WT	1.000	873.2
Δ441-671	96.85	9.015
re1 re2 re3 re4	873.2	1.000
re1 re2 re3 RE4	123.2	7.086
re1 re2 RE3 re4	571.7	1.527
re1 RE2 re3 re4	535.7	1.630
RE1 re2 re3 re4	222.2	3.930
re1 re2 RE3 RE4	3.929	222.3
re1 RE2 re3 RE4	11.52	75.77
re1 RE2 RE3 re4	63.29	13.80
RE1 re2 re3 RE4	3.837	227.6
RE1 re2 RE3 re4	16.78	52.05
RE1 RE2 re3 re4	10.94	79.84
re1 RE2 RE3 RE4	1.107	789.0
RE1 re2 RE3 RE4	1.133	770.6
RE1 RE2 re3 RE4	1.158	754.3
RE1 RE2 RE3 re4	2.635	331.4

<sup>1</sup> Fold Basal Activity Relative to WT CARD11

<sup>2</sup> Fold Basal Activity Relative to CARD11 Quadruple RE mutant

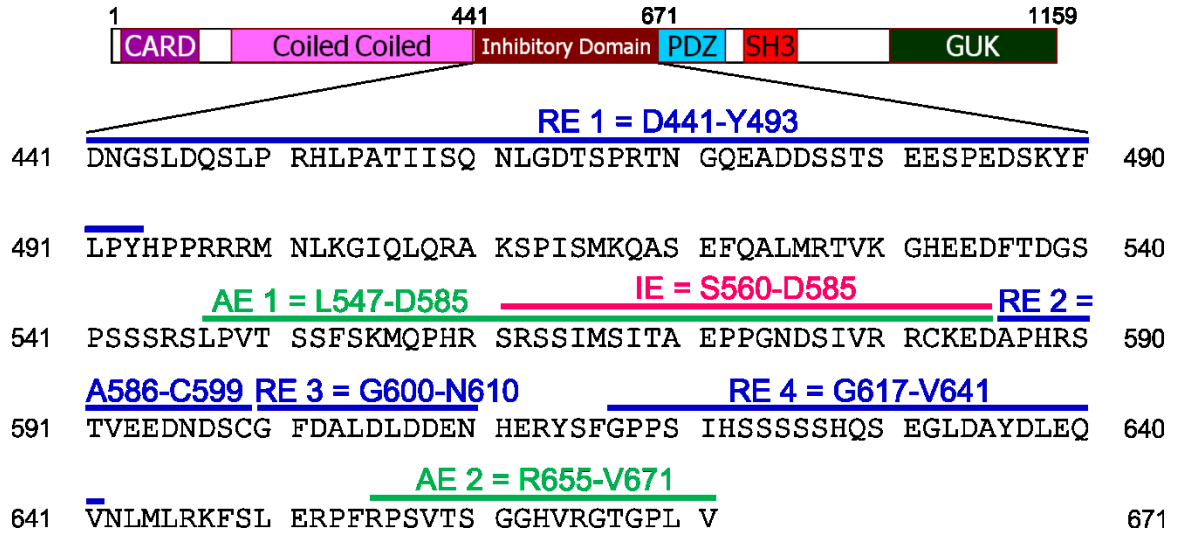


## **Figures and Figure Legends**

### **Figure 2.1: CARD11's inhibitory domain comprises of multiple functional elements.**

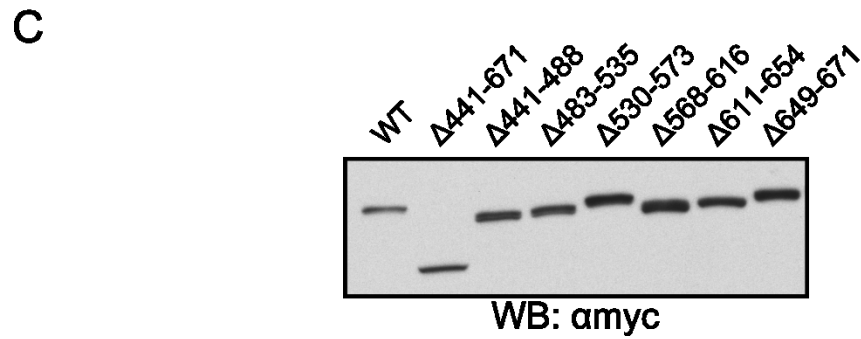
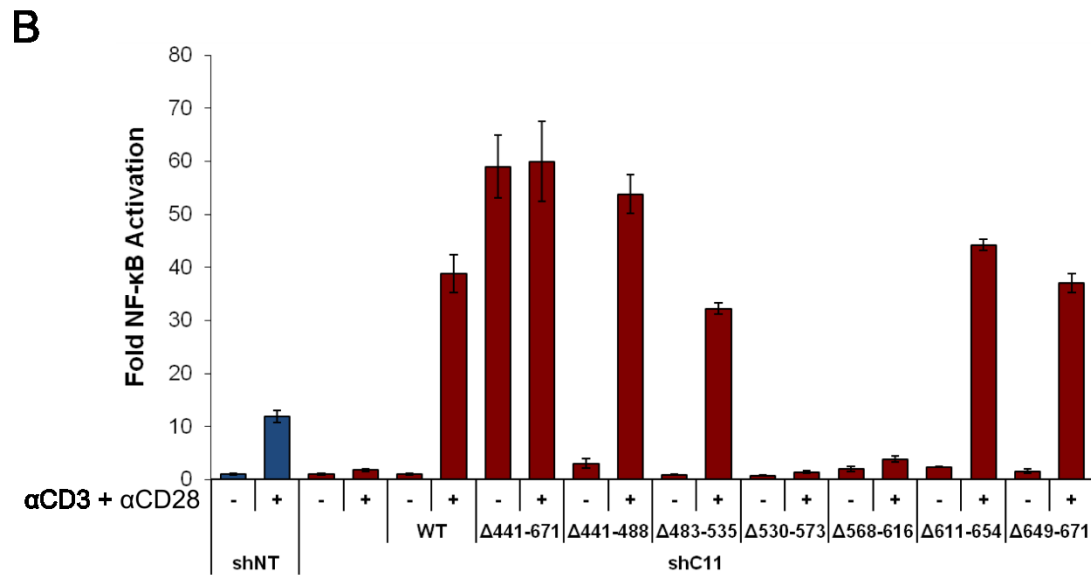
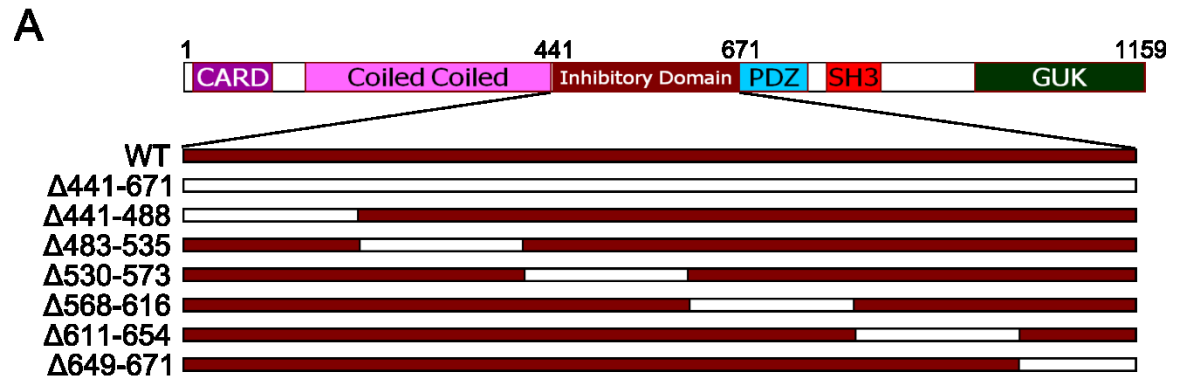
Schematic representation of murine CARD11 protein with enlargement of the residues 441-671 corresponding to CARD11's inhibitory domain. Position and boundaries of four repressive elements, two activating elements and a single inducibility element within the ID are illustrated.

Figure 2.1



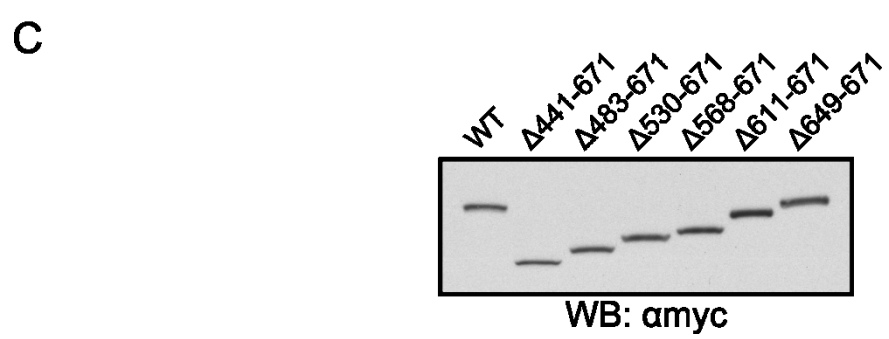
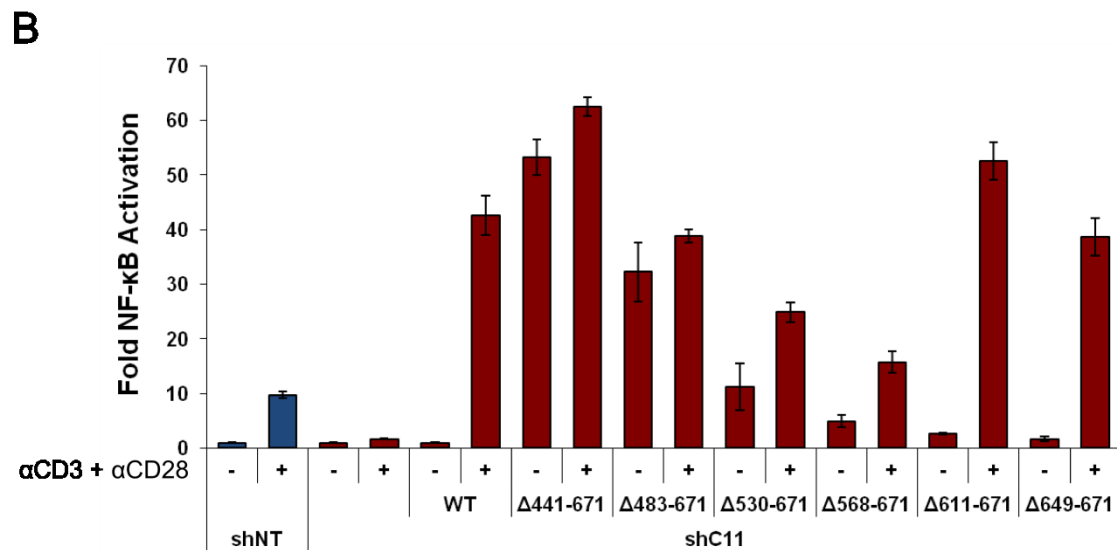
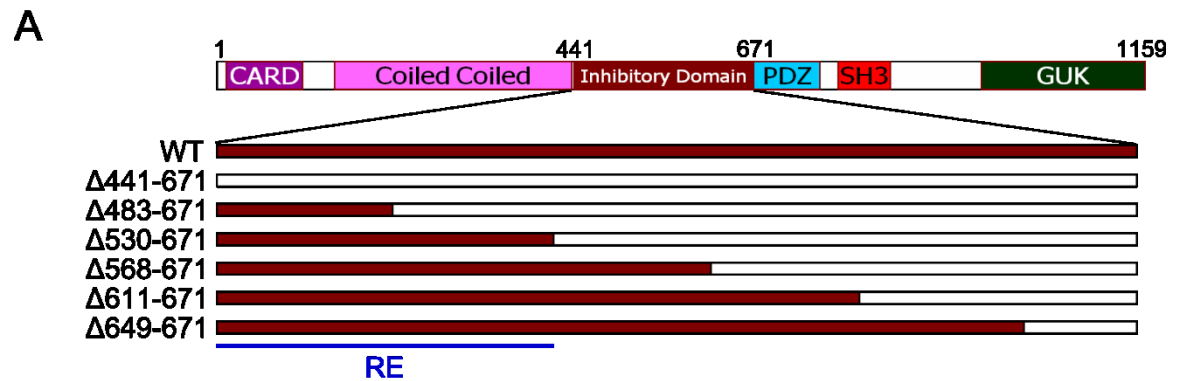
**Figure 2.2: CARD11's inhibitory function consists of multiple regions with repressive function.** (A) Schematic representation of intradomain ID deletions. (B) NF- $\kappa$ B luciferase assay performed on stable CARD11 knockdown Jurkat T cells transfected with indicated murine CARD11 variants and stimulated with 1 $\mu$ g/ml  $\alpha$ CD3, 1 $\mu$ g/ml  $\alpha$ CD28 for 5 hrs. Jurkat T cells stably expressing NT shRNA and CARD11 shRNA transfected without CARD11 rescue constructs were used as controls. (C) 293T expression assay using ng amounts of CARD11 intradomain ID deletion expression constructs transfected in (B) and blotted for anti-myc showed that all constructs are expressed equivalently.

Figure 2.2



**Figure 2.3: N-terminus of ID contains a repressive element.** (A) Schematic representation of CARD11 ID deletion constructs analyzed. Portions of the inhibitory domain are sequentially added from the N-terminus of the ID. (B) NF- $\kappa$ B luciferase assay performed on stable CARD11 knockdown Jurkat T cells transfected with indicated murine CARD11 variants and stimulated with 1 $\mu$ g/ml  $\alpha$ CD3, 1 $\mu$ g/ml  $\alpha$ CD28 for 5 hrs. Jurkat T cells stably expressing NT shRNA and CARD11 shRNA transfected without CARD11 rescue constructs were used as controls. (C) 293T expression assay using ng amounts of CARD11 N-terminal ID addition expression constructs transfected in (B) and blotted for anti-myc showed that all constructs are expressed equivalently.

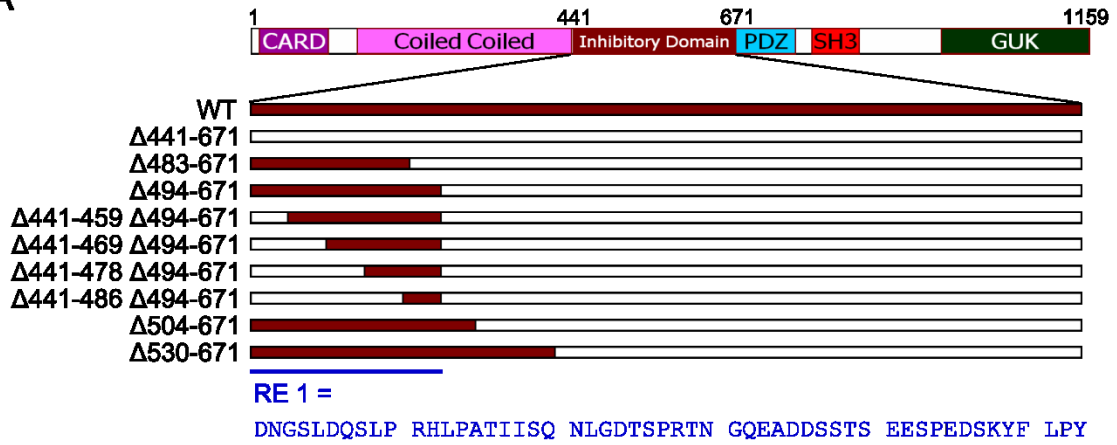
Figure 2.3



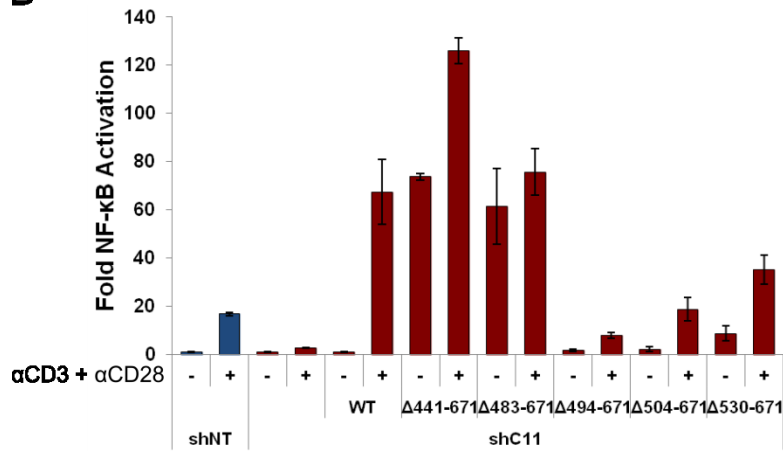
**Figure 2.4: CARD11 RE1 maps to residues 441-493.** (A) Schematic representation of CARD11 ID deletion constructs analyzed. Portions of the putative N-terminal repressive element are deleted from the C-terminus and then deleted from the N-terminus using the identified C-terminal boundary. The sequence of the minimal repressive element is shown. (B, D) NF- $\kappa$ B luciferase assay performed on stable CARD11 knockdown Jurkat T cells transfected with indicated murine CARD11 variants and stimulated with 1 $\mu$ g/ml  $\alpha$ CD3, 1 $\mu$ g/ml  $\alpha$ CD28 for 5 hrs. Jurkat T cells stably expressing NT shRNA and CARD11 shRNA transfected without CARD11 rescue constructs were used as controls. (C) 293T expression assay using ng amounts of CARD11 C-terminal deletion expression constructs transfected in (B) and blotted for anti-myc showed that all constructs are expressed equivalently. (E) 293T expression assay using ng amounts of CARD11 N-terminal deletion expression constructs transfected in (D) and blotted for anti-myc showed that all constructs are expressed equivalently.

Figure 2.4

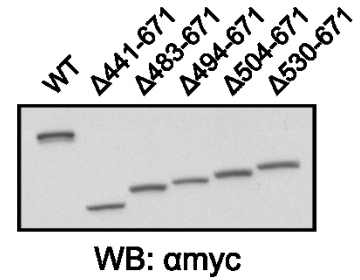
A



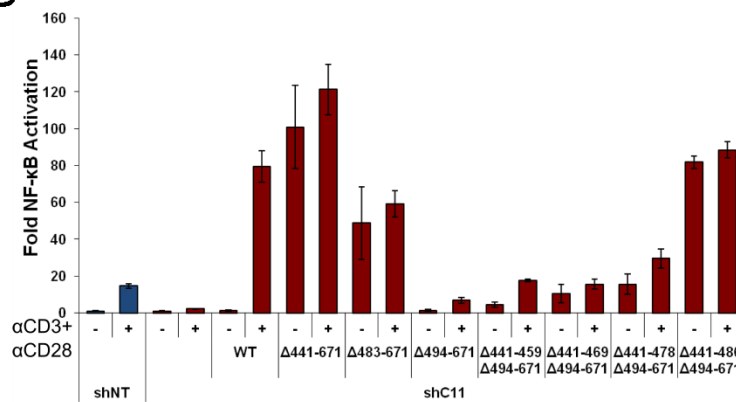
B



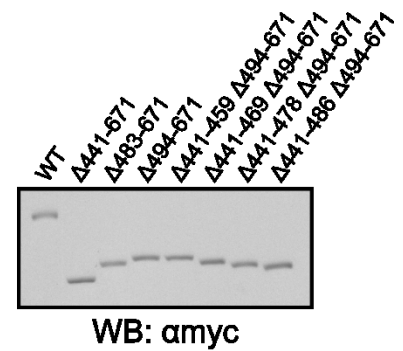
C



D



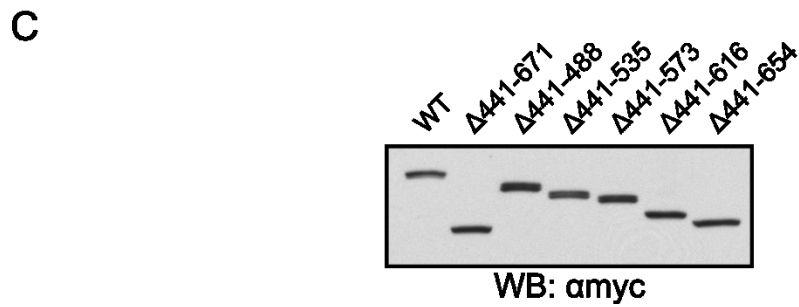
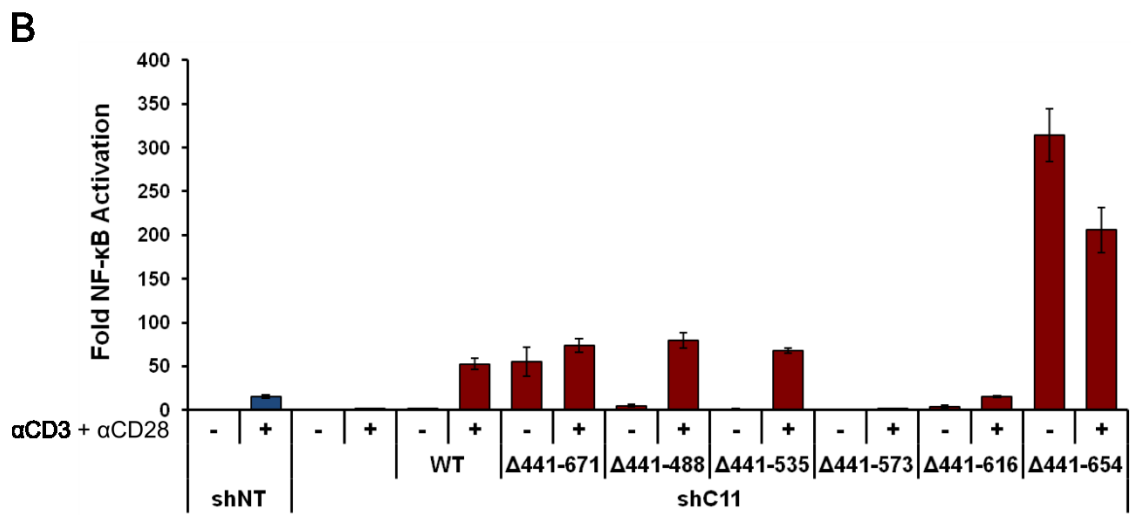
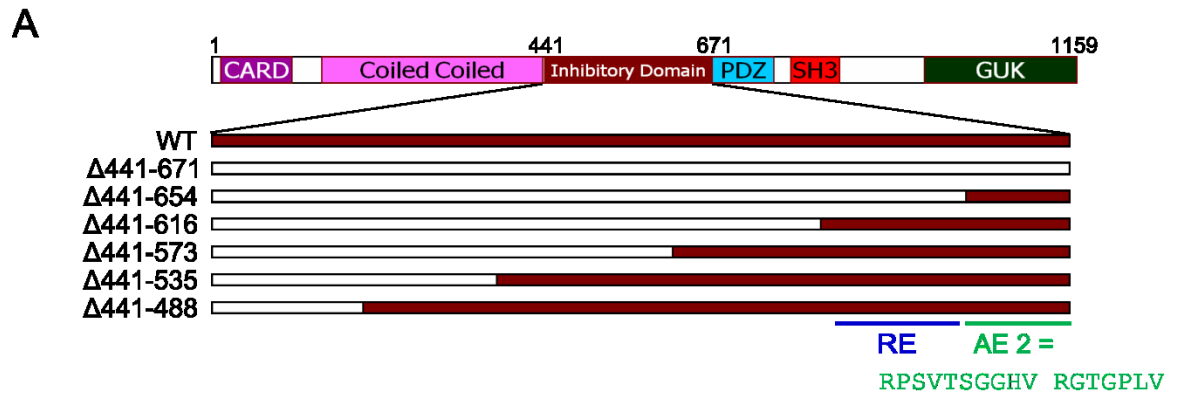
E





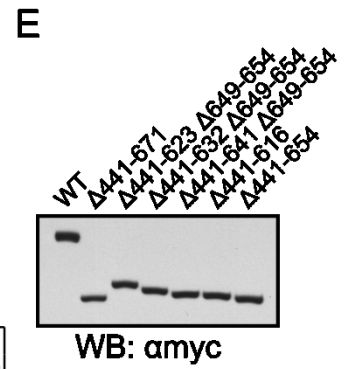
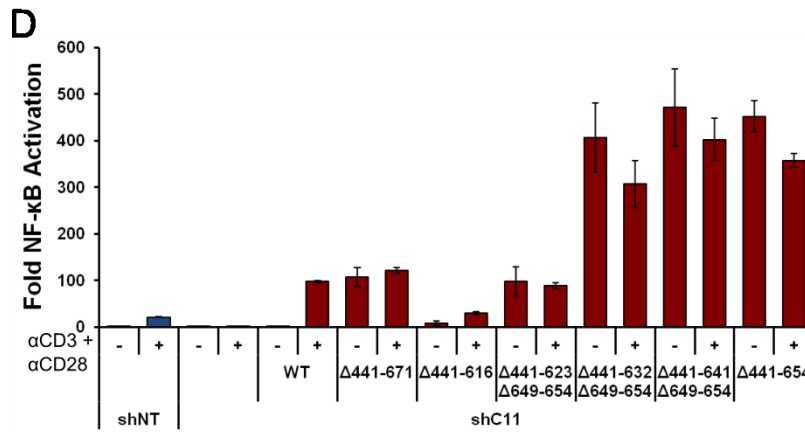
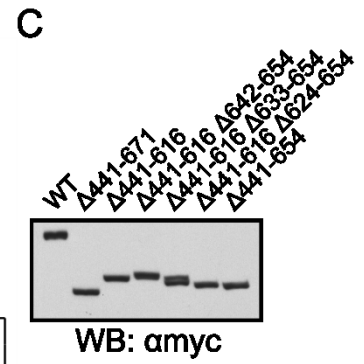
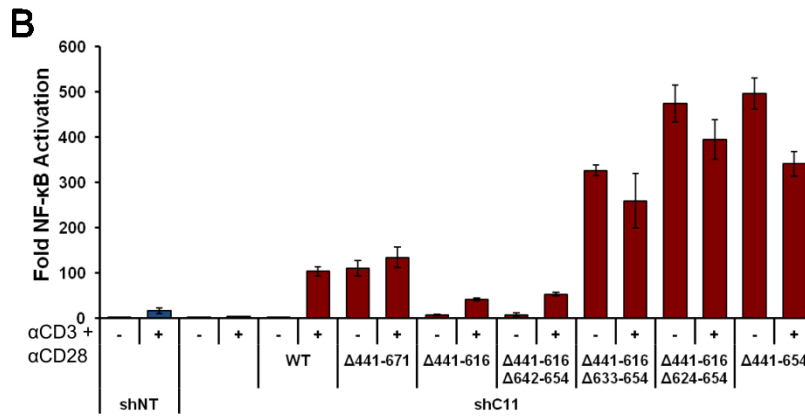
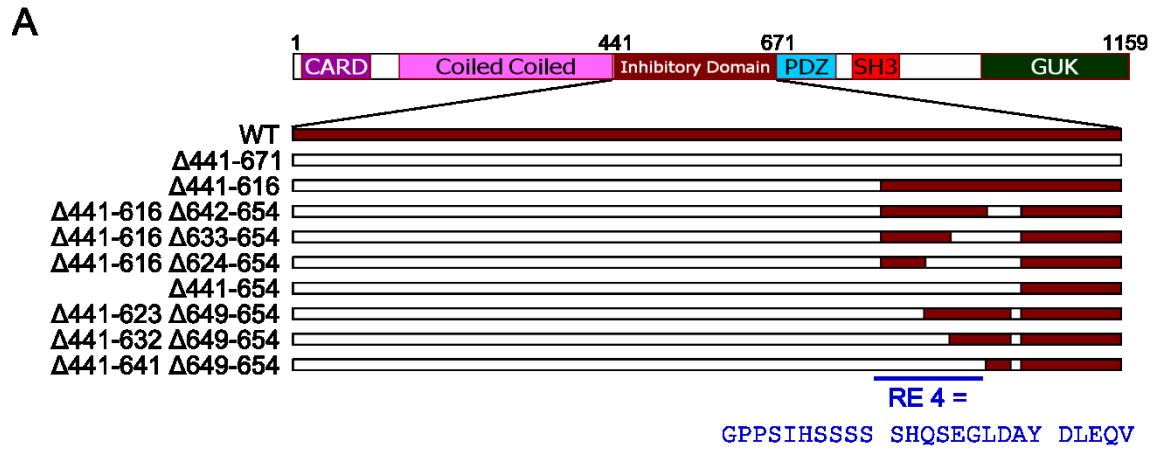
**Figure 2.5: C-terminus of ID contains a novel activating element and a potent repressive element.** (A) Schematic representation of CARD11 ID constructs analyzed. Portions of the inhibitory domain are sequentially added from the C-terminus of the ID. The sequence of the minimal activating element is shown. (B) NF- $\kappa$ B luciferase assay performed on stable CARD11 knockdown Jurkat T cells transfected with indicated murine CARD11 variants and stimulated with 1 $\mu$ g/ml  $\alpha$ CD3, 1 $\mu$ g/ml  $\alpha$ CD28 for 5 hrs. Jurkat T cells stably expressing NT shRNA and CARD11 shRNA transfected without CARD11 rescue constructs were used as controls. (C) 293T expression assay using ng amounts of CARD11 C-terminal addition expression constructs transfected in (B) and blotted for anti-myc showed that all constructs are expressed equivalently.

Figure 2.5



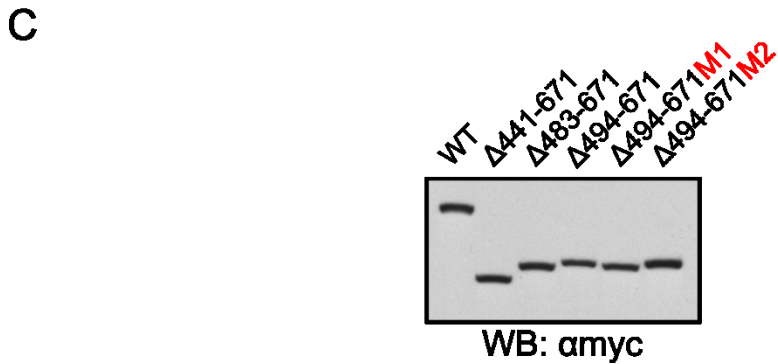
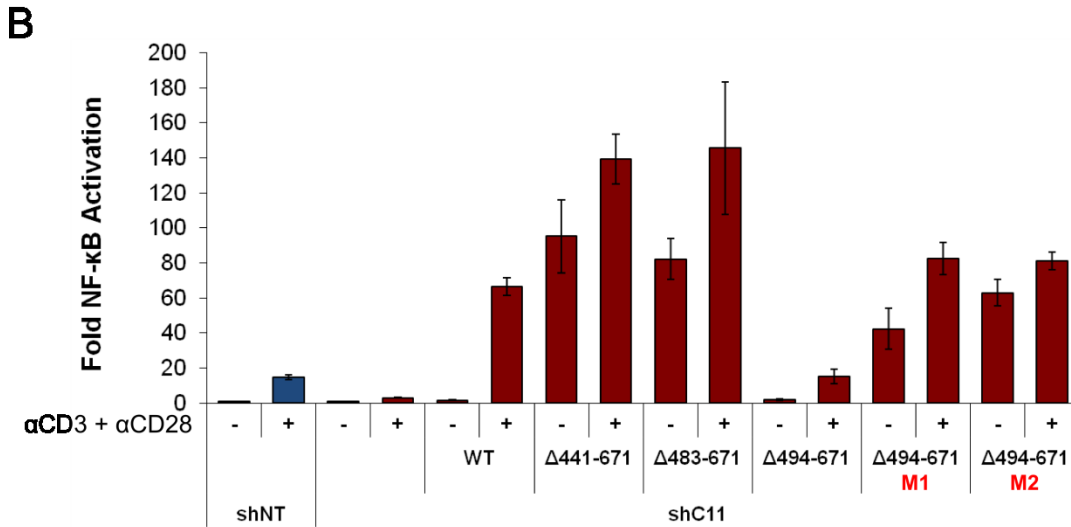
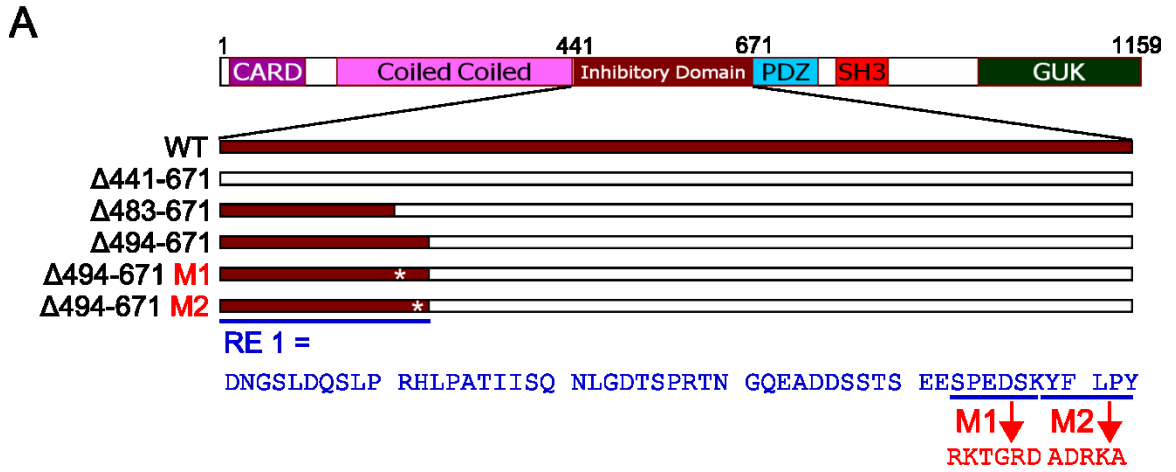
**Figure 2.6: CARD11 RE4 maps to residues 617-641.** (A) Schematic representation of CARD11 ID deletion constructs analyzed. Portions of the inhibitory domain are deleted from C- or N-terminus of the putative RE4 without affecting AE2. The sequence of the minimal repressive element is shown. (B, D) NF- $\kappa$ B luciferase assay performed on stable CARD11 knockdown Jurkat T cells transfected with indicated murine CARD11 variants and stimulated with 1 $\mu$ g/ml  $\alpha$ CD3, 1 $\mu$ g/ml  $\alpha$ CD28 for 5 hrs. Jurkat T cells stably expressing NT shRNA and CARD11 shRNA transfected without CARD11 rescue constructs were used as controls. (C) 293T expression assay using ng amounts of the indicated CARD11 expression constructs transfected in (B) and blotted for anti-myc showed that all constructs are expressed equivalently. (E) 293T expression assay using ng amounts of the indicated CARD11 expression constructs transfected in (D) and blotted for anti-myc showed that all constructs are expressed equivalently.

Figure 2.6



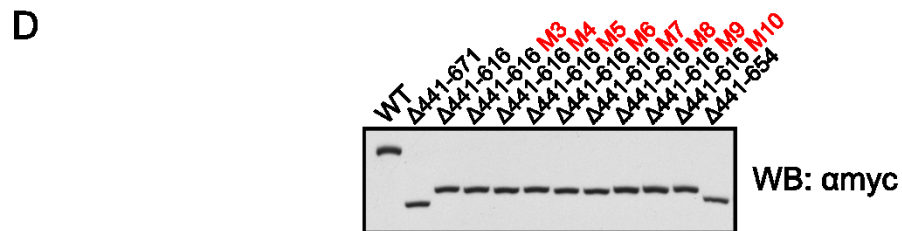
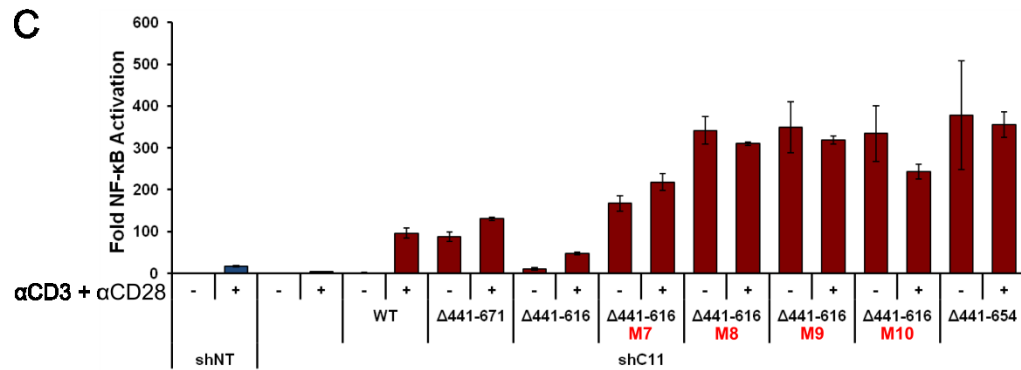
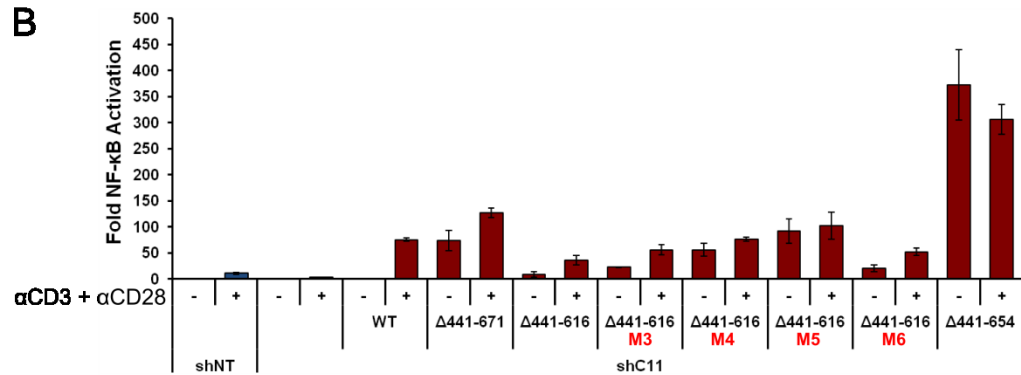
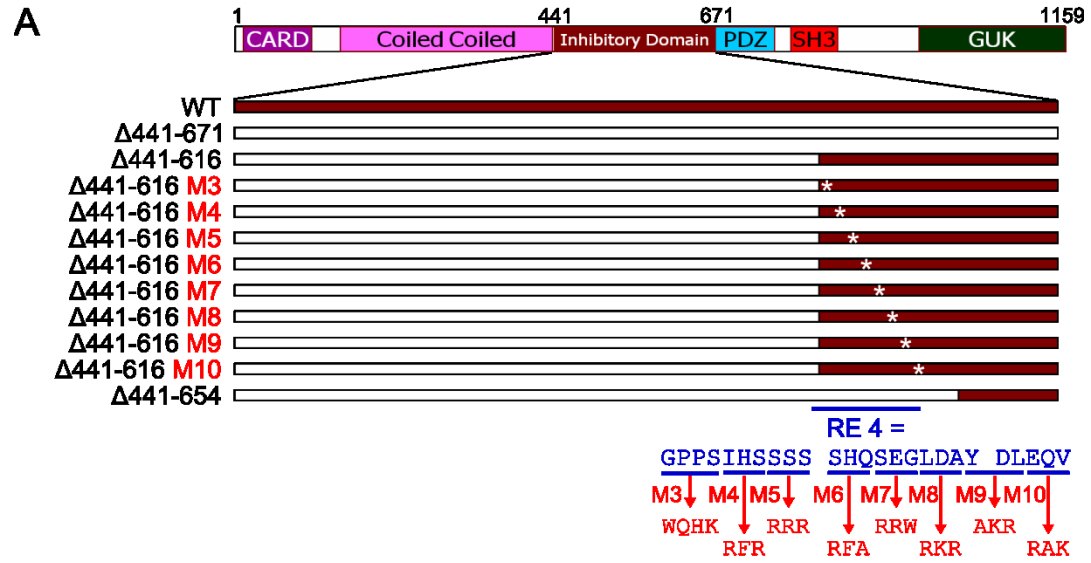
**Figure 2.7: M1 and M2 abolish RE1 repressive function.** (A) Schematic representation of CARD11 minimal RE1 and mutant variant constructs analyzed. (B) NF- $\kappa$ B luciferase assay performed on stable CARD11 knockdown Jurkat T cells transfected with indicated murine CARD11 variants and stimulated with 1 $\mu$ g/ml  $\alpha$ CD3, 1 $\mu$ g/ml  $\alpha$ CD28 for 5 hrs. Jurkat T cells expressing NT shRNA and stable CARD11 knockdown cells transfected without CARD11 rescue constructs were used as controls. (C) 293T expression assay using ng amounts of CARD11 RE1 variant expression constructs transfected in (B) and blotted for anti-myc showed that all constructs are expressed equivalently.

Figure 2.7



**Figure 2.8: Multiple mutations in RE4 disrupt its repression.** (A) Schematic representation of CARD11 RE4 and mutant variant constructs analyzed. (B, C) NF- $\kappa$ B luciferase assay performed on stable CARD11 knockdown Jurkat T cells transfected with indicated murine CARD11 variants and stimulated with 1 $\mu$ g/ml  $\alpha$ CD3, 1 $\mu$ g/ml  $\alpha$ CD28 for 5 hrs. Jurkat T cells stably expressing NT shRNA and CARD11 shRNA transfected without CARD11 rescue constructs were used as controls. (D) 293T expression assay using ng amounts of CARD11 RE4 variant expression constructs transfected in (B and C) and blotted for anti-myc showed that all constructs are expressed equivalently.

Figure 2.8

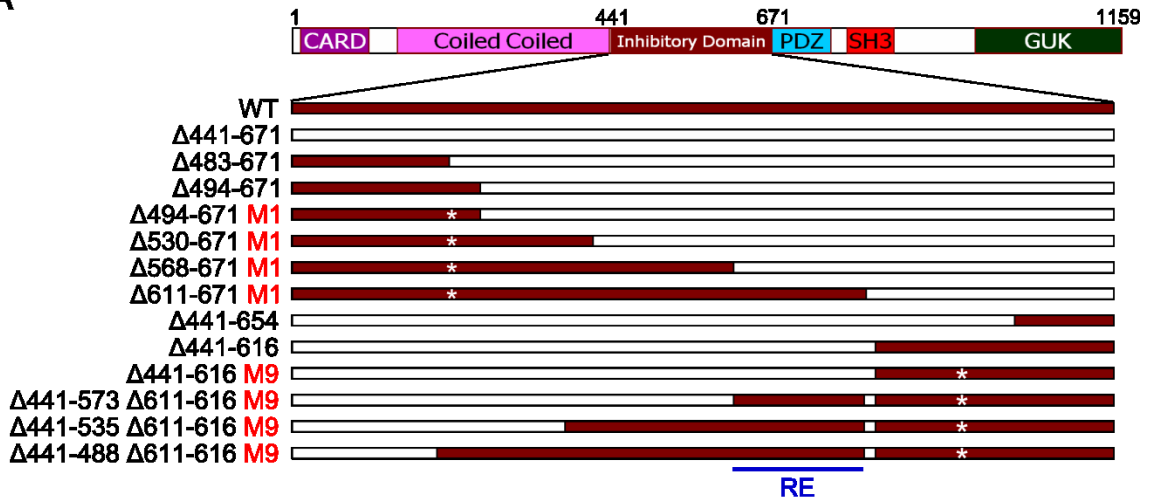




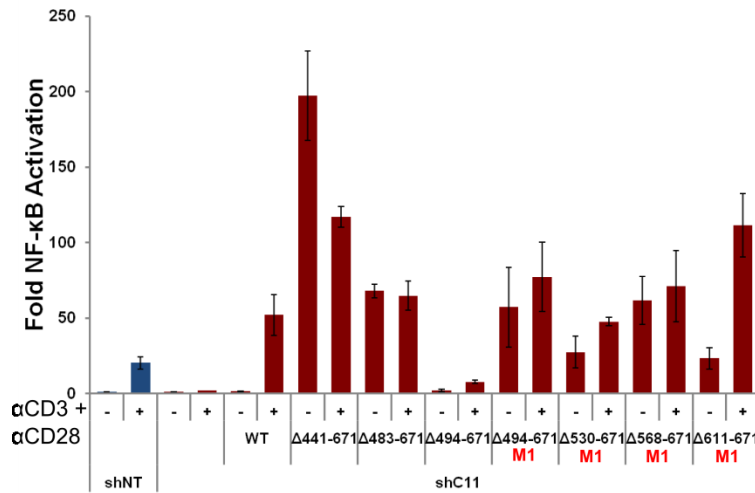
**Figure 2.9: Internal regions of the ID include at least one additional repressive element.** (A) Schematic representation of CARD11 ID C-terminal addition constructs in the context of mutating RE1 or CARD11 N-terminal addition constructs in the context of mutating RE4. (B, D) NF- $\kappa$ B luciferase assay performed on stable CARD11 knockdown Jurkat T cells transfected with indicated murine CARD11 variants and stimulated with 1 $\mu$ g/ml  $\alpha$ CD3, 1 $\mu$ g/ml  $\alpha$ CD28 for 5 hrs. Jurkat T cells stably expressing NT shRNA and CARD11 shRNA transfected without CARD11 rescue constructs were used as controls. (C) 293T expression assay using ng amounts of CARD11 C-terminal addition expression constructs in the context of mutating RE1 transfected in (B) and blotted for anti-myc showed that all constructs are expressed equivalently. (E) 293T expression assay using ng amounts of CARD11 N-terminal addition expression constructs in the context of mutating RE4 transfected in (D) and blotted for anti-myc showed that all constructs are expressed equivalently.

# Figure 2.9

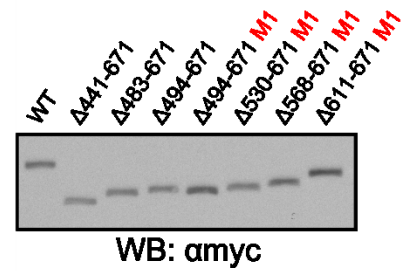
A



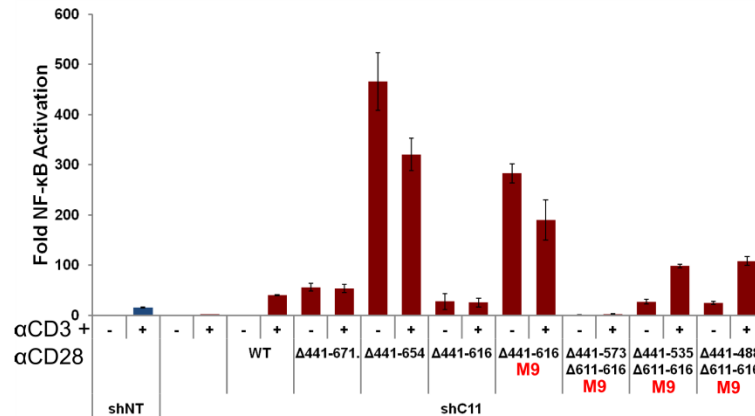
B



C



D



E

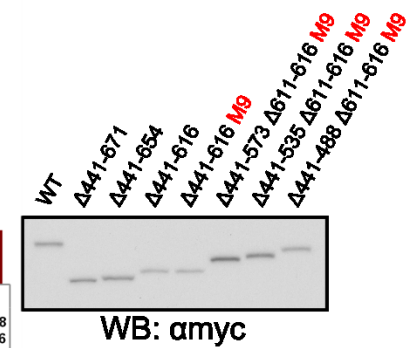


Figure 2.9 courtesy of Julia Tritapoe

**Figure 2.10: CARD11 RE2 and RE3 share homologous sequences that abrogate repression when mutated.** (A) Schematic representation of CARD11 ID N-terminal additions of two independent REs in the context of mutant RE4. The sequence of the two minimal repressive elements is shown. A schematic of RE2 and/or RE3 mutants and their sequence are also shown. (B) NF- $\kappa$ B luciferase assay performed on stable CARD11 knockdown Jurkat T cells transfected with indicated murine CARD11 variants and stimulated with 1 $\mu$ g/ml  $\alpha$ CD3, 1 $\mu$ g/ml  $\alpha$ CD28 for 5 hrs. Jurkat T cells stably expressing NT shRNA and CARD11 shRNA transfected without CARD11 rescue constructs were used as controls. (C) 293T expression assay using ng amounts of specified CARD11 expression constructs transfected in (B) and blotted for anti-myc showed that all constructs are expressed equivalently.

Figure 2.10

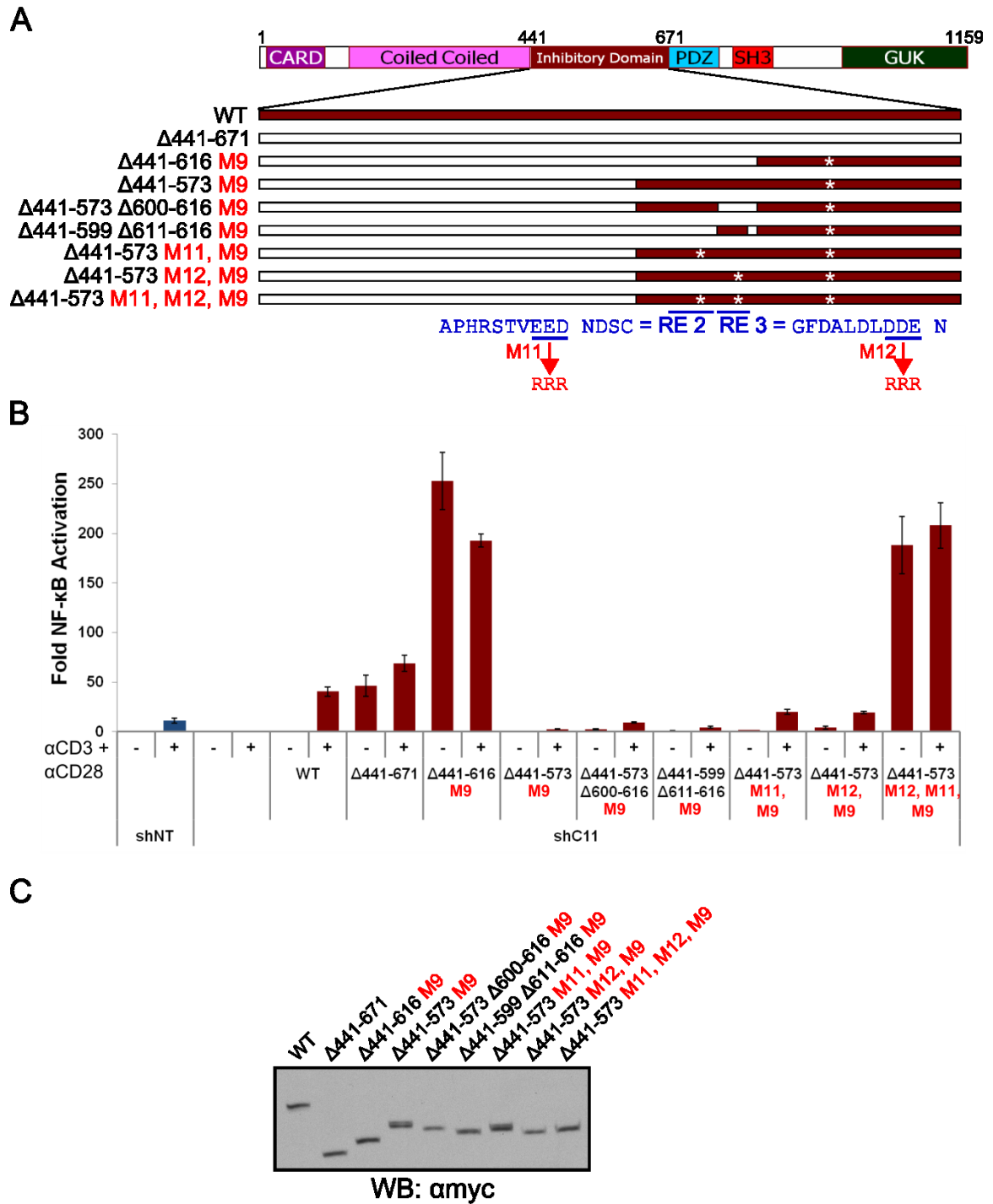
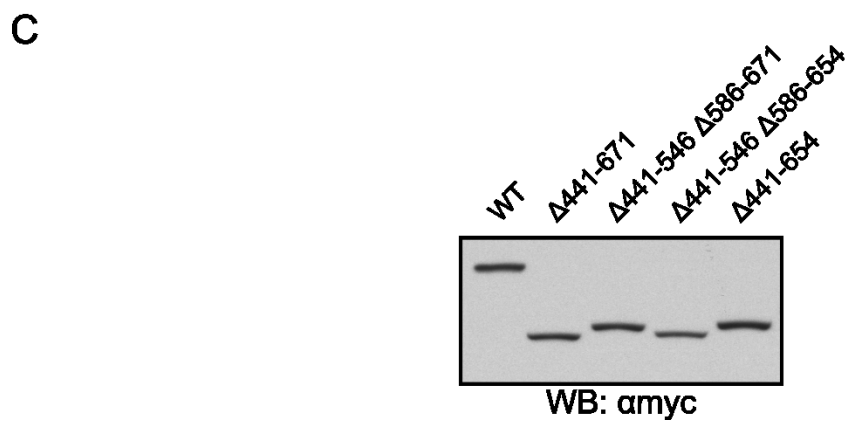
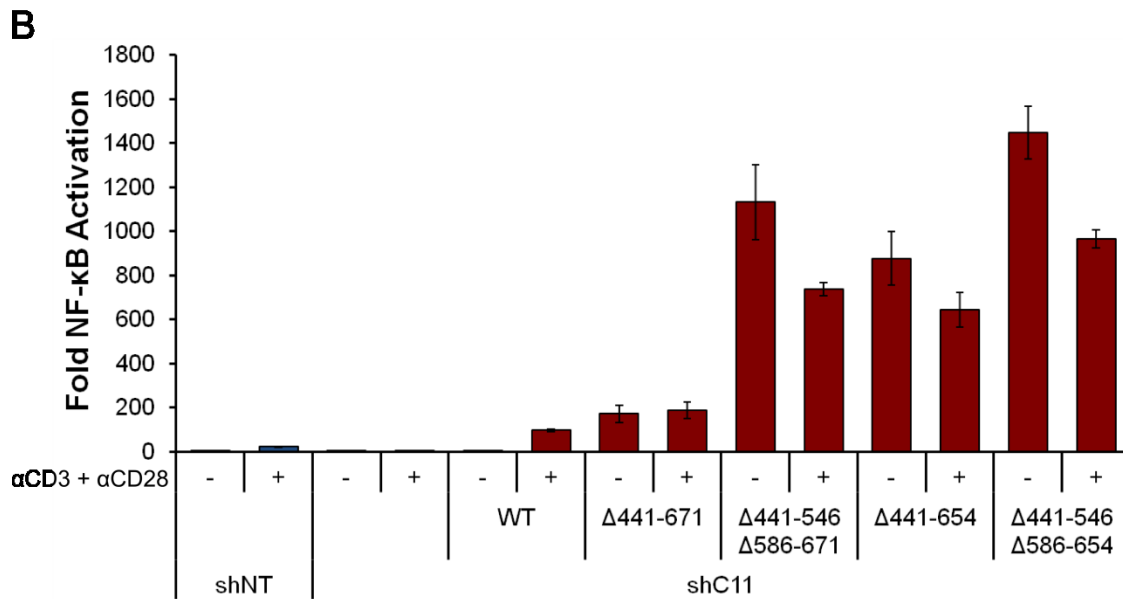
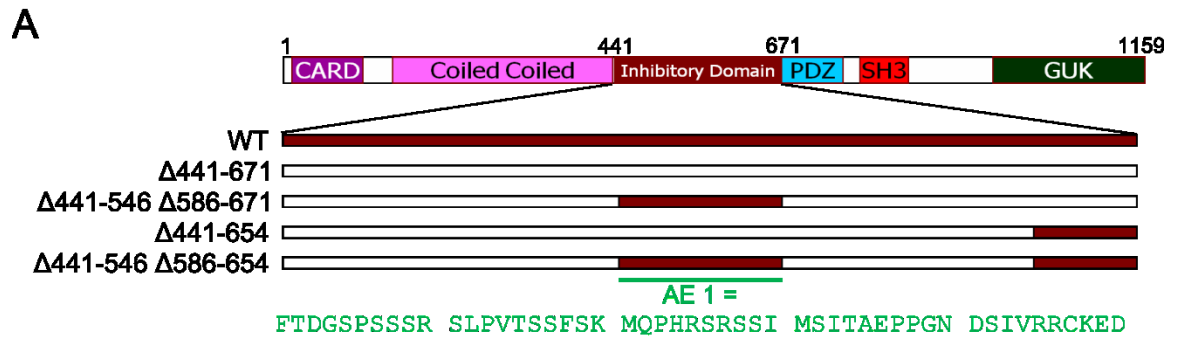


Figure 2.10 courtesy of Julia Tritapoe

**Figure 2.11: CARD11 ID encodes a second activating element.** (A) Schematic representation of CARD11 ID AE1 and/or AE2 constructs analyzed. The sequence of the minimal AE1 is shown. (B) NF- $\kappa$ B luciferase assay performed on stable CARD11 knockdown Jurkat T cells transfected with indicated murine CARD11 variants and stimulated with 1 $\mu$ g/ml  $\alpha$ CD3, 1 $\mu$ g/ml  $\alpha$ CD28 for 5 hrs. Jurkat T cells stably expressing NT shRNA and CARD11 shRNA transfected without CARD11 rescue constructs were used as controls. (C) 293T expression assay using ng amounts of CARD11 AE expression constructs transfected in (B) and blotted for anti-myc showed that all constructs are expressed equivalently.

Figure 2.11



**Figure 2.12: CARD11's inducibility element is embedded within activating element1.** (A) Schematic representation of CARD11 ID internal deletion constructs analyzed. The sequence of the minimal IE is shown. (B) NF- $\kappa$ B luciferase assay performed on stable CARD11 knockdown Jurkat T cells transfected with indicated murine CARD11 variants and stimulated with 1 $\mu$ g/ml  $\alpha$ CD3, 1 $\mu$ g/ml  $\alpha$ CD28 for 5 hrs. Jurkat T cells stably expressing NT shRNA and CARD11 shRNA transfected without CARD11 rescue constructs were used as controls. (C) 293T expression assay using ng amounts of CARD11 internal deletion expression constructs transfected in (B) and blotted for anti-myc showed that all constructs are expressed equivalently.

Figure 2.12

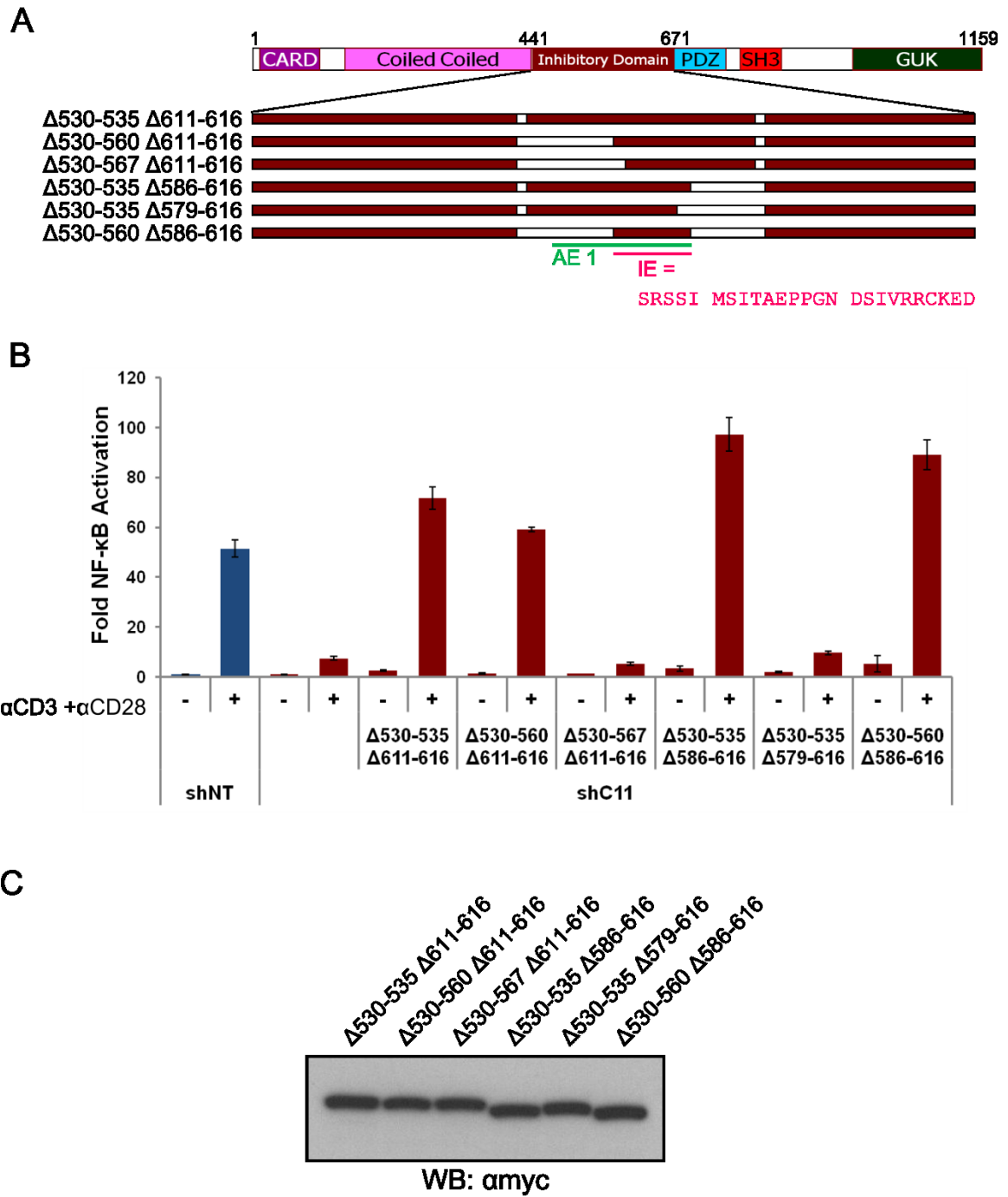
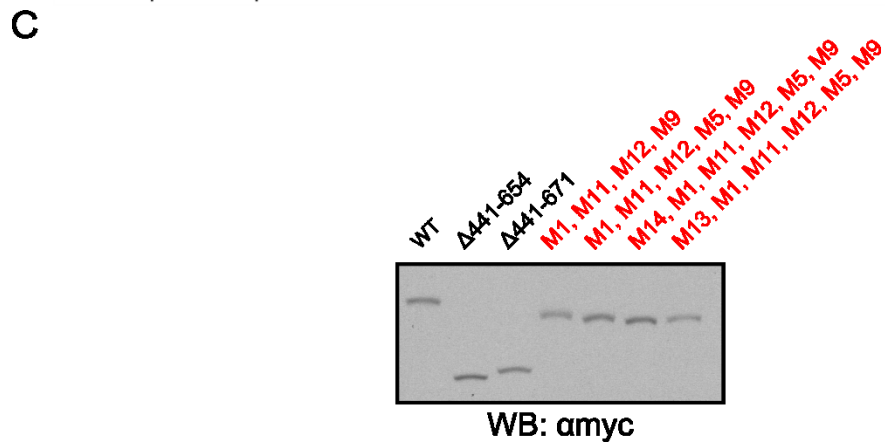
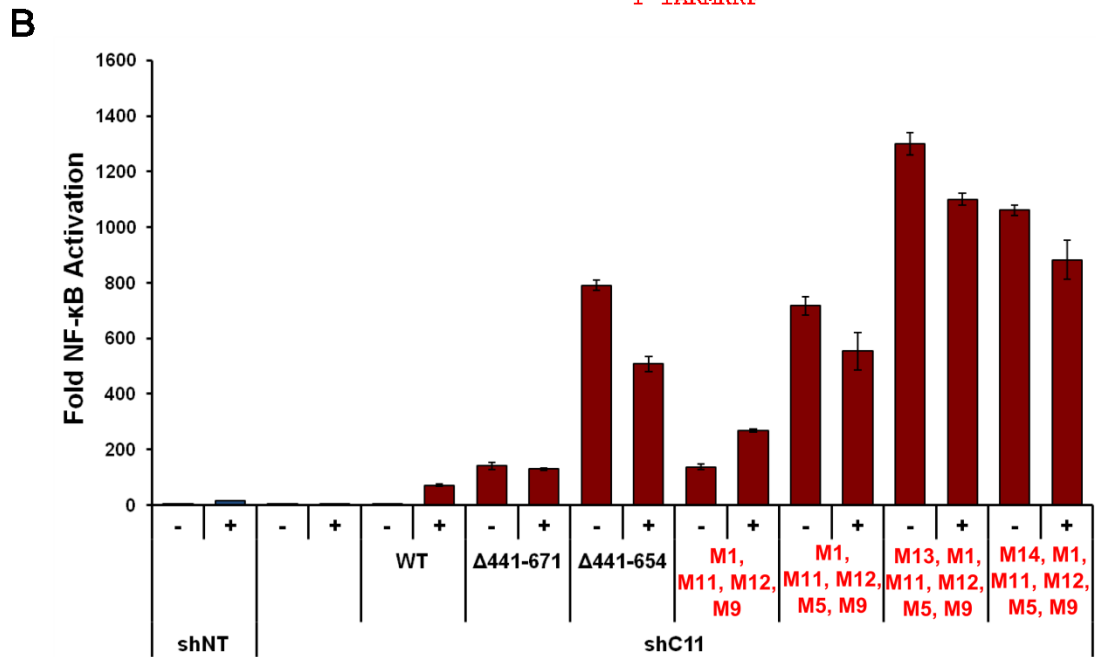
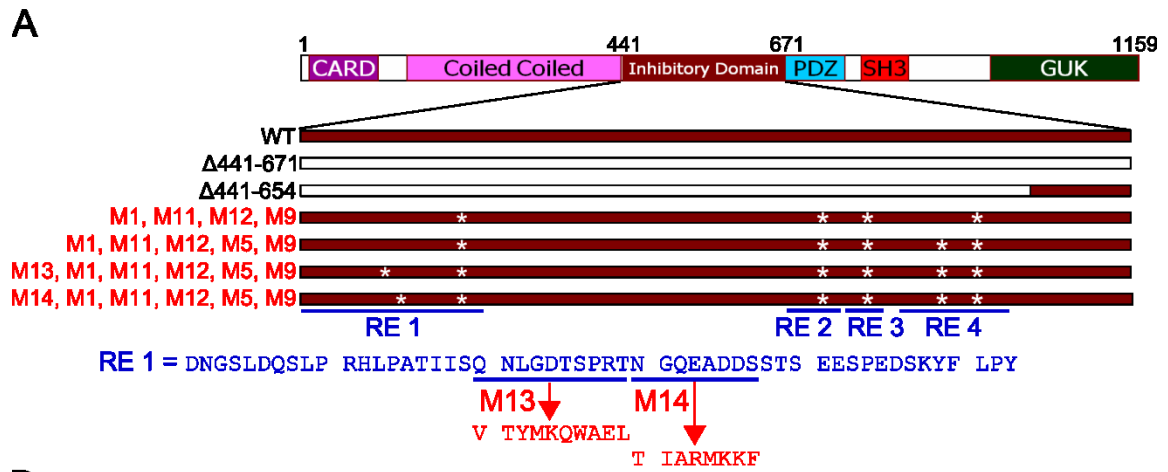


Figure 2.12 courtesy of Julia Tritapoe



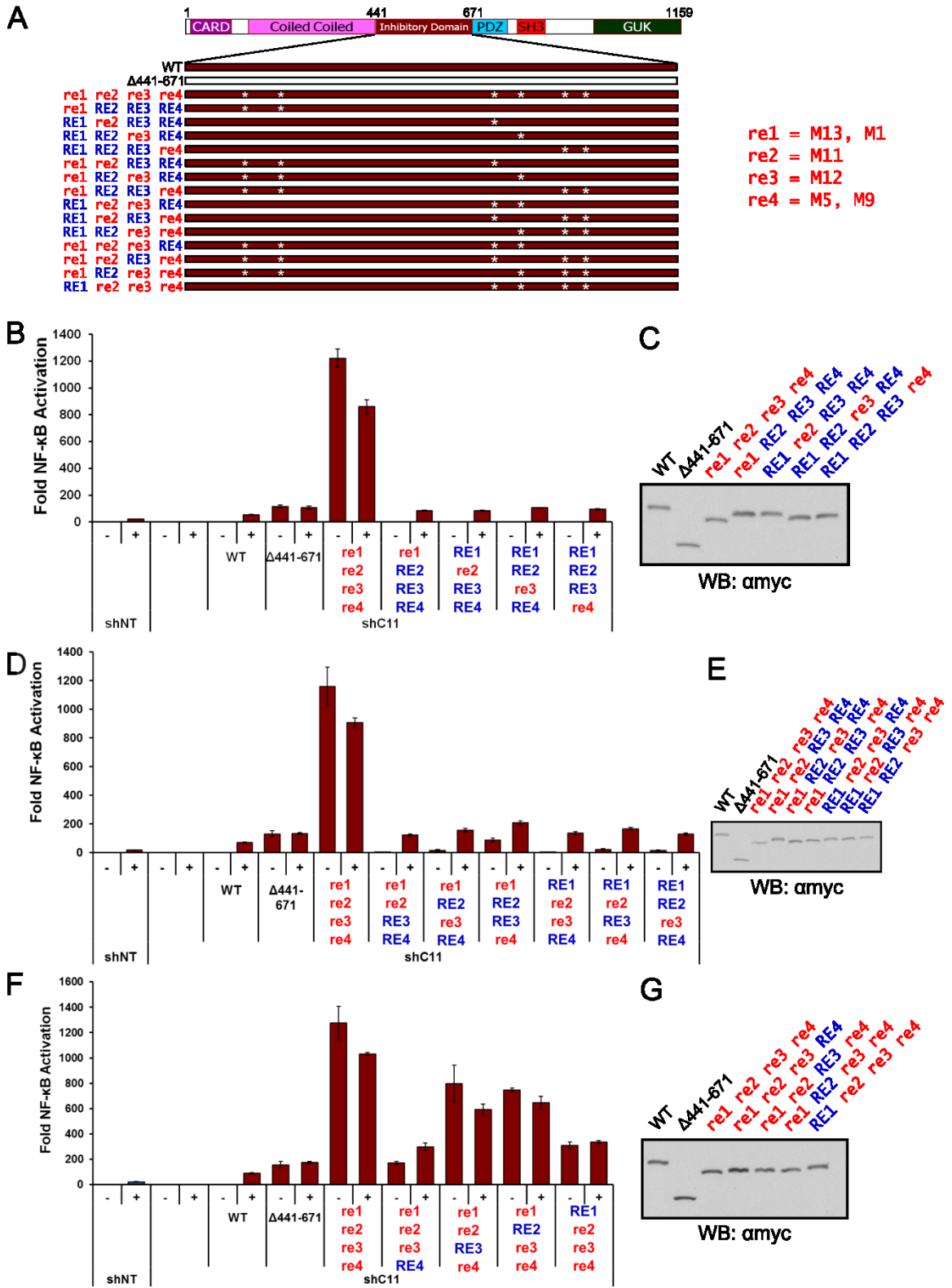
**Figure 2.13: Multiple mutations in multiple repressive elements are required to completely destroy inhibitory function.** (A) Schematic representation of CARD11 full-length quadruple RE mutant variants. Second site mutations M13 and M14 in RE1 are shown. (B) NF- $\kappa$ B luciferase assay performed on stable CARD11 knockdown Jurkat T cells transfected with indicated murine CARD11 variants and stimulated with 1  $\mu$ g/ml  $\alpha$ CD3, 1  $\mu$ g/ml  $\alpha$ CD28 for 5 hrs. Jurkat T cells stably expressing NT shRNA and CARD11 shRNA transfected without CARD11 rescue constructs were used as controls. (C) 293T expression assay using ng amounts of CARD11 quadruple RE mutant expression constructs transfected in (B) and blotted for anti-myc showed that all constructs are expressed equivalently.

Figure 2.13



**Figure 2.14: Repressive elements act synergistically to repressive basal NF- $\kappa$ B activity.** (A) Schematic representation of CARD11 full-length single, double or triple RE mutant variants. (B) NF- $\kappa$ B luciferase assay performed on stable CARD11 knockdown Jurkat T cells transfected with indicated murine single RE mutant CARD11 variants and stimulated with 1 $\mu$ g/ml  $\alpha$ CD3, 1 $\mu$ g/ml  $\alpha$ CD28 for 5 hrs. Jurkat T cells stably expressing NT shRNA and CARD11 shRNA transfected without CARD11 rescue constructs were used as controls. (C) 293T expression assay using ng amounts of CARD11 single RE mutant variant expression constructs transfected in (B) and blotted for anti-myc showed that all constructs are expressed equivalently. (D) NF- $\kappa$ B luciferase assay performed on stable CARD11 knockdown Jurkat T cells transfected with indicated murine double RE mutant CARD11 variants and stimulated with 1 $\mu$ g/ml  $\alpha$ CD3, 1 $\mu$ g/ml  $\alpha$ CD28 for 5 hrs. Jurkat T cells stably expressing NT shRNA and CARD11 shRNA transfected without CARD11 rescue constructs were used as controls. (E) 293T expression assay using ng amounts of CARD11 double RE mutant variant expression constructs transfected in (D) and blotted for anti-myc showed that all constructs are expressed equivalently. (F) NF- $\kappa$ B luciferase assay performed on stable CARD11 knockdown Jurkat T cells transfected with indicated murine triple RE mutant CARD11 variants and stimulated with 1 $\mu$ g/ml  $\alpha$ CD3, 1 $\mu$ g/ml  $\alpha$ CD28 for 5 hrs. Jurkat T cells stably expressing NT shRNA and CARD11 shRNA transfected without CARD11 rescue constructs were used as controls. (G) 293T expression assay using ng amounts of CARD11 triple RE mutant variant expression constructs transfected in (F) and blotted for anti-myc showed that all constructs are expressed equivalently.

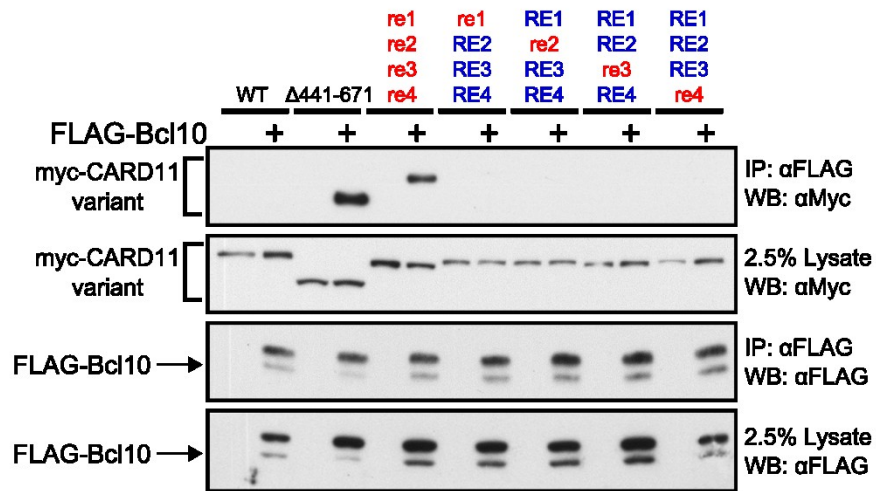
Figure 2.14



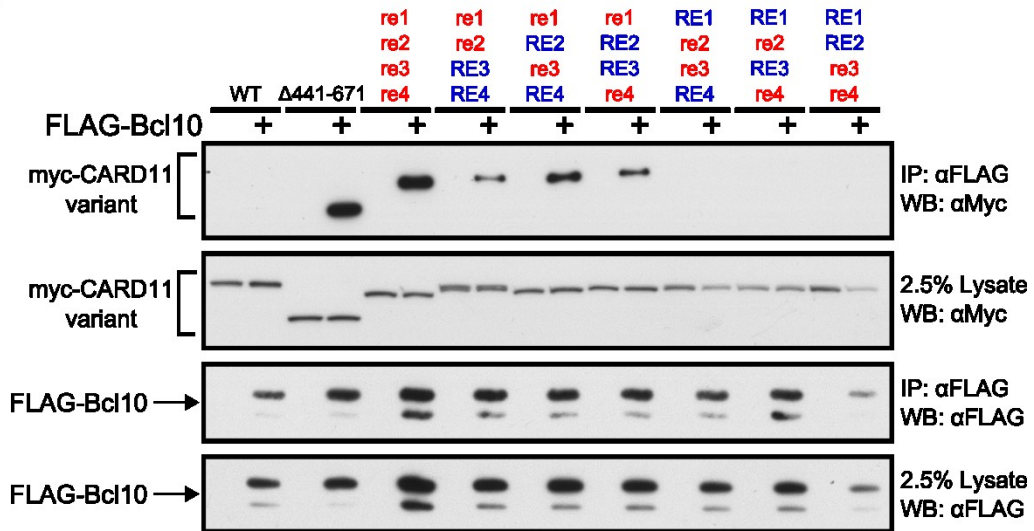
**Figure 2.15: All repressive elements work together to prevent Bcl10 association.** (A-C) HEK 293T cells transfected with the indicated myc-CARD11 variants in the absence of presence of FLAG-tagged Bcl10 were subjected to anti-FLAG co-immunoprecipitation. Co-IP of FLAG-Bcl10 and myc-CARD11 WT or ID-deleted variants were used as negative and positive controls, respectively.

Figure 2.15

A



B



C

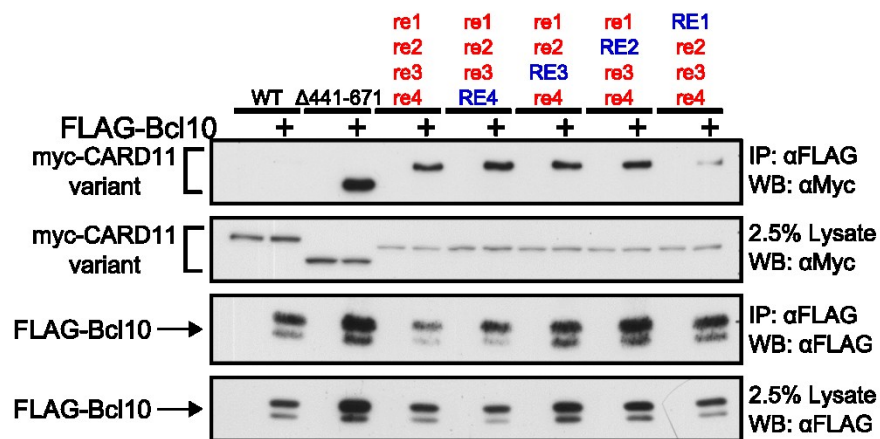
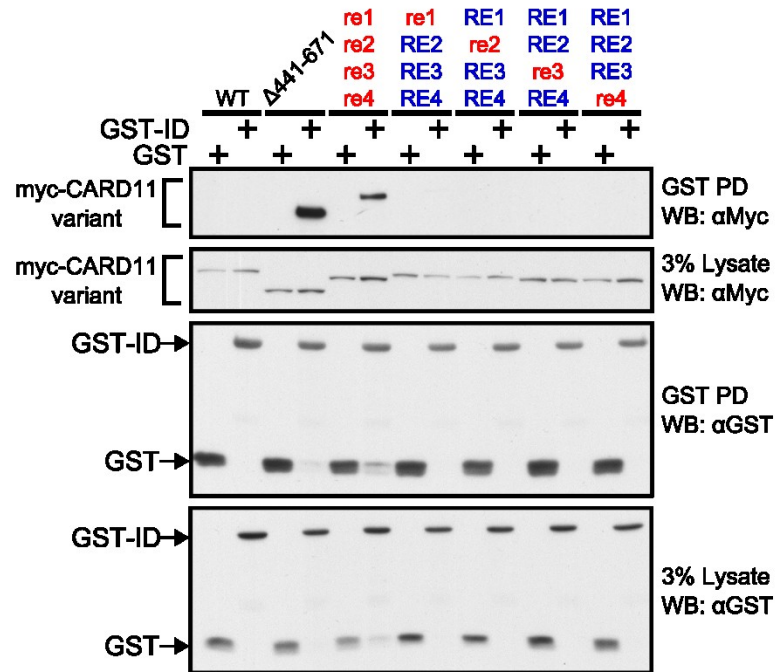


**Figure 2.16: Multiple repressive elements control intramolecular binding. (A-C)**  
HEK 293T cells were co-transfected with indicated Myc-CARD11 variant and either FLAG-GST-ID or FLAG-GST expression constructs. Lysates were pulled down with Glutathione Sepharose beads.

Figure 2.16

A



B

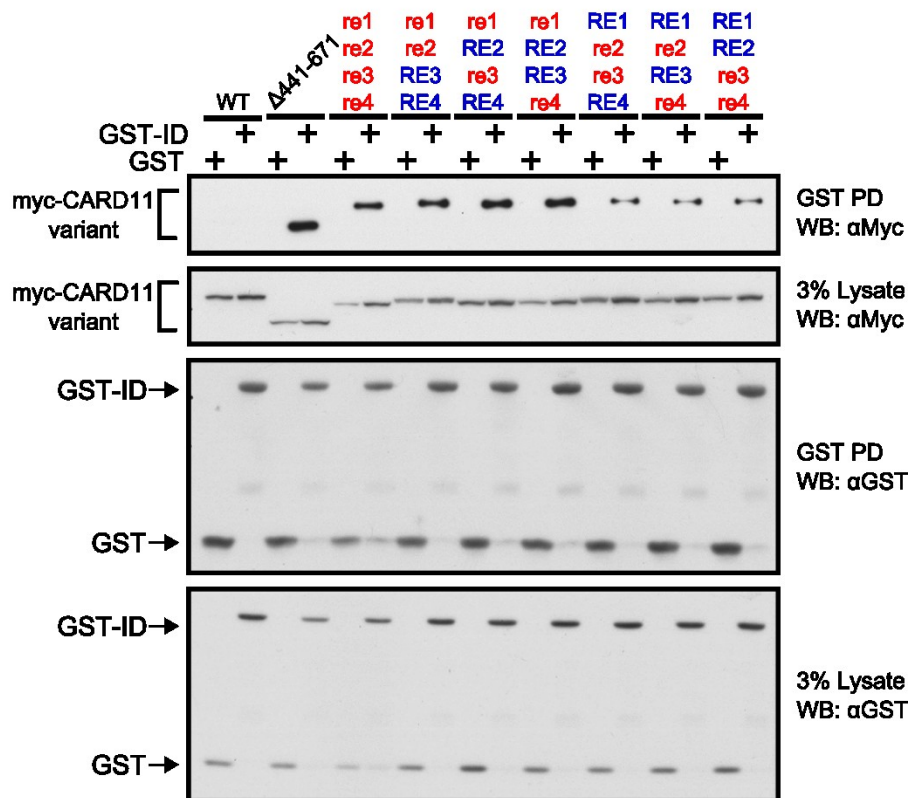
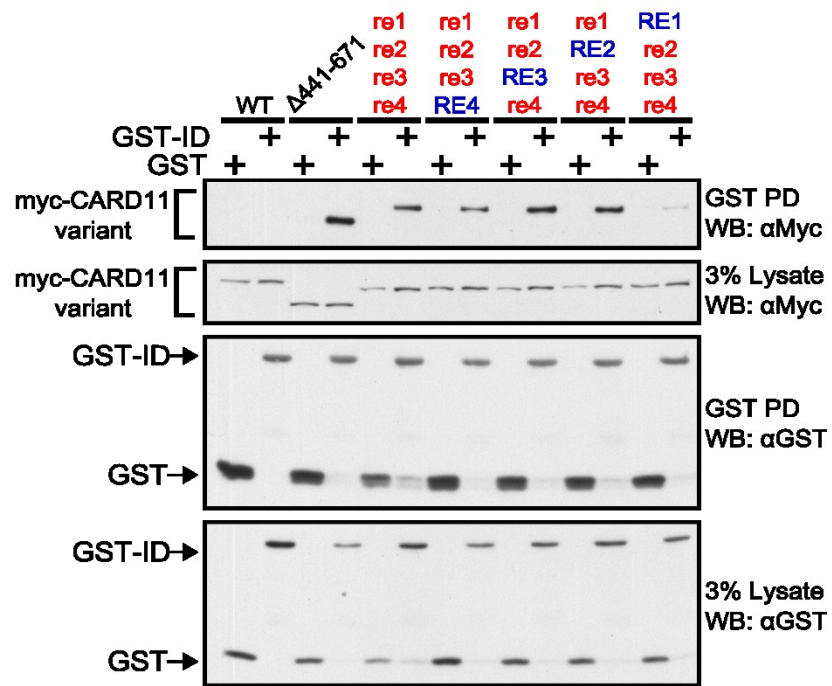




Figure 2.16 cont.

C



**Figure 2.17: Isolated repressive elements are sufficient to bind to other domains within CARD11.** (A-D) GST pulldown of HEK 293T cells co-transfected with the following expression constructs: myc-CARD11 WT, single RE1 mutant and  $\Delta$ ID with FLAG-GST or FLAG-GST-RE1<sub>4</sub> (A); myc-CARD11 WT, single RE2 mutant and  $\Delta$ ID with FLAG-GST or FLAG-GST-RE2<sub>4</sub> (B); myc-CARD11 WT, single RE3 mutant and  $\Delta$ ID with FLAG-GST or FLAG-GST-RE3<sub>4</sub> (C); myc-CARD11 WT, single RE4 mutant and  $\Delta$ ID with FLAG-GST or FLAG-GST-RE4<sub>4</sub> (D).

Figure 2.17

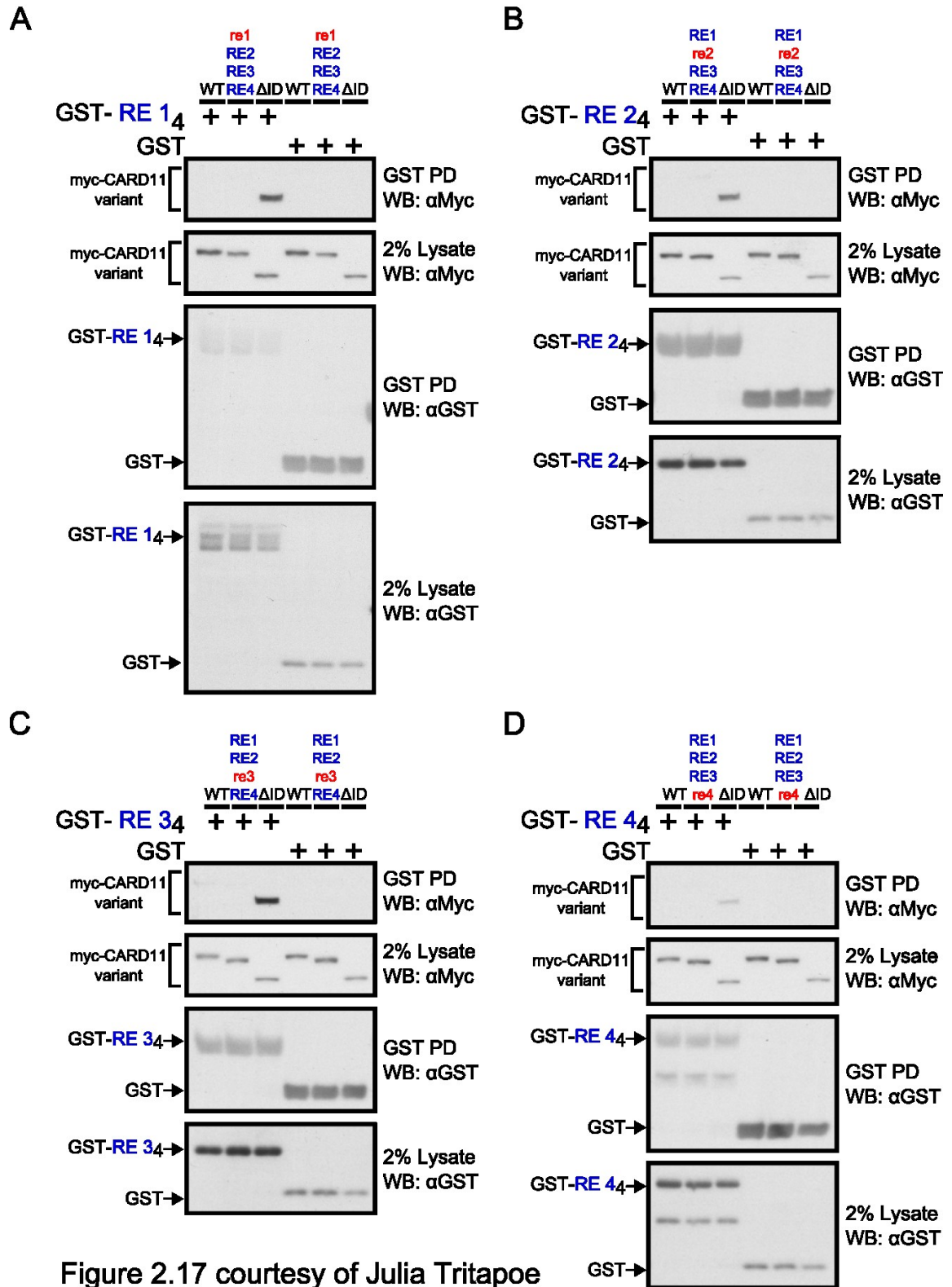


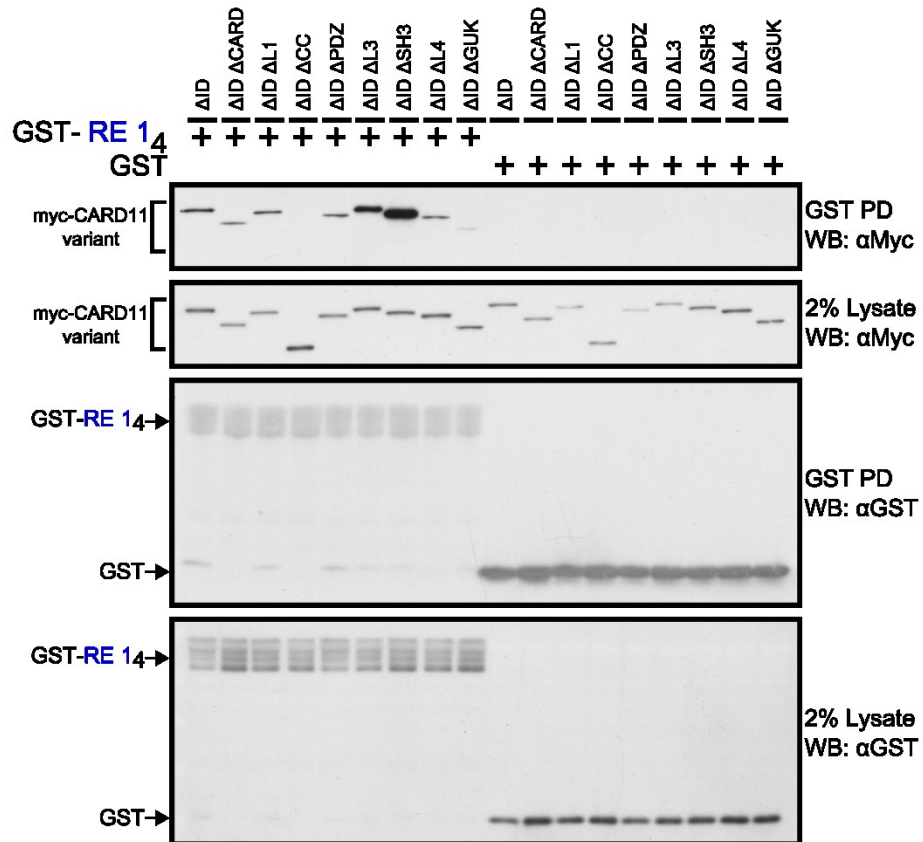
Figure 2.17 courtesy of Julia Tritapoe

**Figure 2.18: Repressive elements 1, 2 and 3 bind to different domains of CARD11.**

(A-C) HEK 293T cells co-transfected with the indicated myc-CARD11  $\Delta$ ID deletion variant and FLAG-GST or the following FLAG-GST-RE<sub>4</sub> variants were subjected to GST PD: FLAG-GST-RE1<sub>4</sub> (A), FLAG-GST-RE2<sub>4</sub> (B), FLAG-GST-RE3<sub>4</sub> (C).

Figure 2.18

A



B

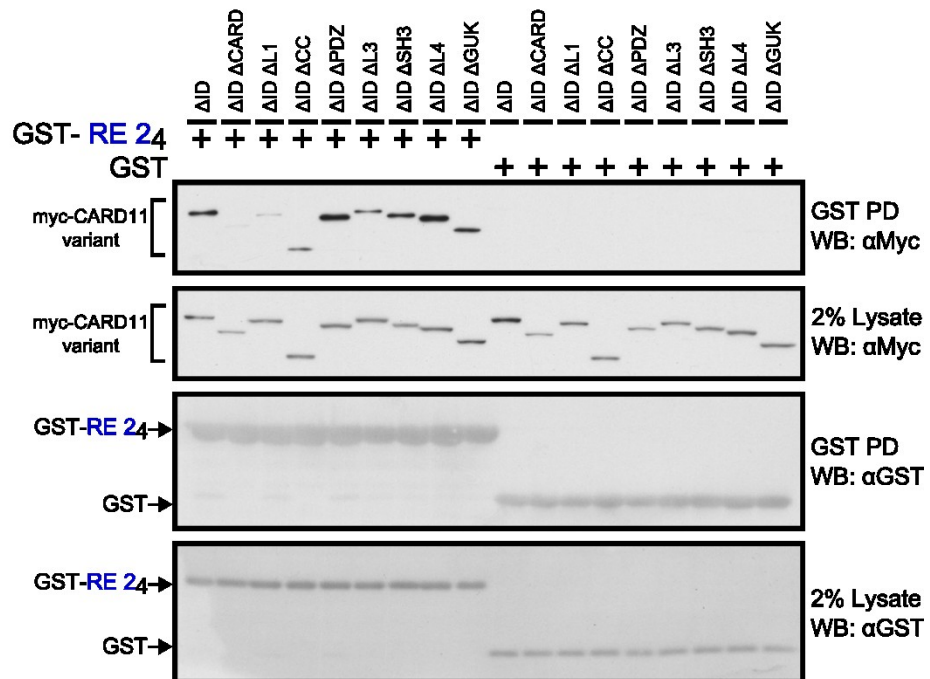


Figure 2.18 cont.

C

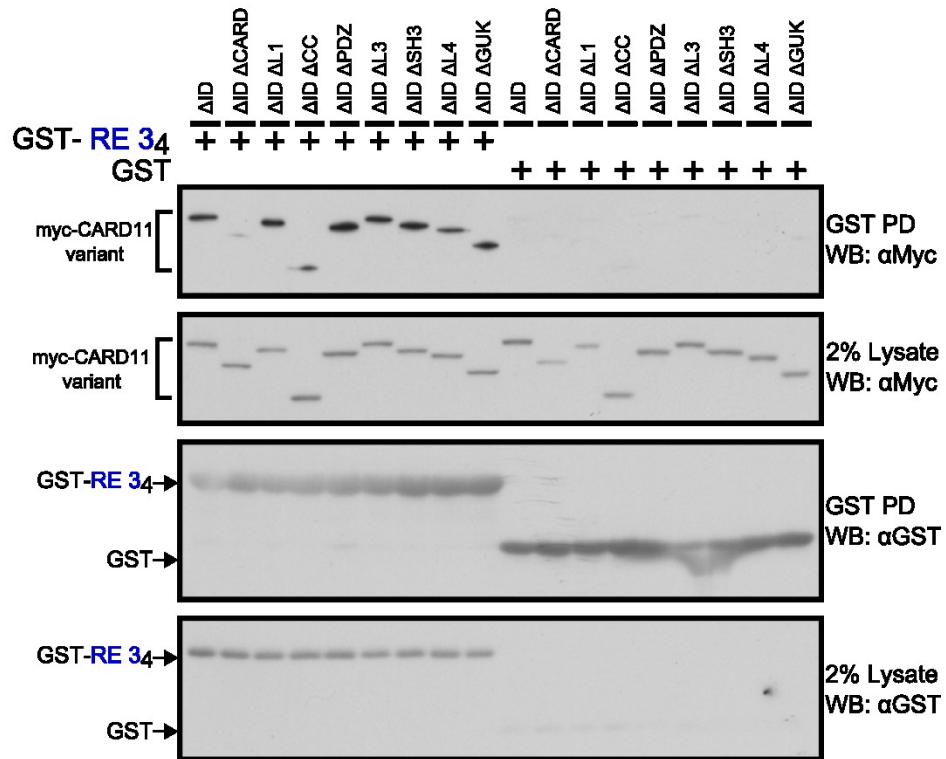


Figure 2.18 courtesy of Julia Tritapoe

**Figure 2.19: Oncogenic CARD11 mutations disrupt binding to multiple ID repressive elements.** (A-C) Indicated Myc-CARD11  $\Delta$ ID oncogenic variants were co-transfected with FLAG-GST, FLAG-GST-RE1<sub>4</sub> (A), FLAG-GST-RE2<sub>4</sub> (B), or FLAG-GST-RE3<sub>4</sub> (C) into HEK 293T. Cell lysates were incubated with Glutathione Sepharose beads.

Figure 2.19

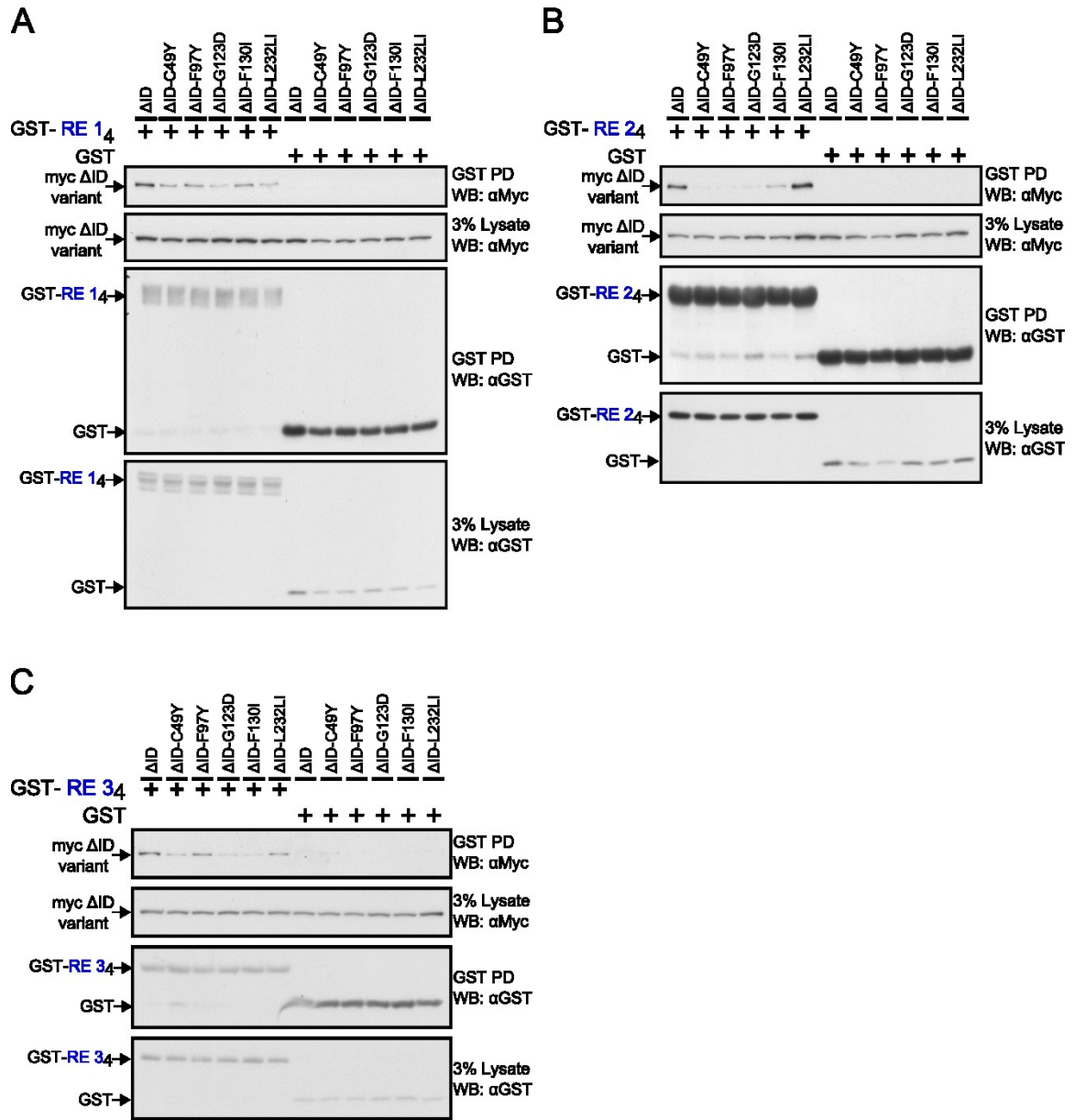


Figure 2.19C courtesy of Julia Tritapoe



## **Chapter III: Discussion**

CARD11 autoinhibition by its ID is essential for controlling intramolecular interactions, scaffolding function and downstream NF- $\kappa$ B activation. Exactly how the ID inhibits activity before antigen receptor engagement and triggers the transition into the active conformation is poorly understood. Our results revealed that the inhibitory domain actually contains multiple modulating elements that cooperatively control CARD11 activity and output. Among these elements, four independent repressive elements act redundantly to keep CARD11 in the closed, inactive conformation and prevent Bcl10 association. Each RE binds a unique set of intramolecular sites that partially overlap. Furthermore, RE inhibition is neutralized by a single, central inducibility element. The overall CARD11 activity is determined by the interplay between the previous elements and two newly identified activating elements. The lymphoma-associated CARD, LATCH and CC domain mutants manipulate this regulatory dynamic by undoing the effects of at least two ID REs.

While the four REs were functionally and mechanistically redundant, they had unique properties. Aside from RE2 and RE3, there was very little sequence similarity among the REs in terms of length and amino acid composition (Figure 2.1). These differences most likely account for the different potencies of each RE (Table 2.4). Despite the fact that all four REs were capable of inhibiting Bcl10 binding and maintaining intramolecular contacts, RE1 appeared to be the most effective for both. In fact, all three other REs needed to be mutated to see appreciable binding to Bcl10 (Figure 2.15C). Though all four REs were sufficient to bind the remaining CARD11 domains, RE4 binding was barely detectable (Figure 2.17D). Similarly, the three REs required

different domains to mediate this binding (Figure 2.18). Thus, each RE had a distinct repressive profile.

Though previous studies only implicated the CARD, L1 and CC in ID binding, we found an additional requirement of the GUK domain to bind RE1 (Figure 2.18A) (Chan et al., 2013; McCully and Pomerantz, 2008). Our results also implicated the L3 and SH3 domains as inhibitors of RE1 binding. This result is not surprising given evidence in the literature of the SH3 domains of other MAGUK family members binding intramolecularly with their GUK domain and possibly occluding GUK accessibility (McGee and Brecht, 1999; Pan et al., 2011; Qian and Prehoda, 2006). It is generally thought that GUK domains are important for protein-protein interactions; however, little is understood about GUK domain function in CARD11 activation (Li et al., 2002; Oliva et al., 2012). Previous studies showed the GUK domain was required for Ag-mediated NF- $\kappa$ B activation and for constitutive PP2A constant regulatory subunit A (PPP2R1A) binding (Eitelhuber et al., 2011; Pomerantz et al., 2002). Interestingly, PP2A negatively regulates CARD11-mediated NF- $\kappa$ B activity by dephosphorylating S657 (Eitelhuber et al., 2011). Hence, it is possible that RE1 mediates PP2A binding to the GUK domain or regulates the inhibitory function of PP2A. Similarly, RE1 may regulate the negative regulator PKC $\delta$ , which binds the MAGUK of CARD11 (Liu et al., 2012). Because previous studies also showed that the adapter protein ADAP binds the MAGUK moiety of CARD11 to activate downstream NF- $\kappa$ B activity in T cells, RE1 could instead compete with ADAP and lead to repression (Medeiros et al., 2007). Further studies are needed to determine if there is a link between RE1 and PP2A and/or ADAP.

One intriguing question our studies tried to address is how intramolecular interactions are related to Bcl10 binding. It is possible that disruption of RE binding must precede Bcl10 binding, and the two repressive mechanisms are separable. Alternatively, a decrease in RE binding may cause obligatory Bcl10 binding without a second regulatory step. A third possibility is that Bcl10 binding competes for the same RE binding sites and displaces the RE. With the exception of the CARD11 double mutants variants where RE1 is WT, all RE mutant variants that disrupt intramolecular binding are also able to bind Bcl10 (Figure 2.15 and Figure 2.16). Although in most cases there is a negative correlation between intramolecular binding and Bcl10 association, this result suggests that disrupting RE binding may not automatically dictate Bcl10 binding. We cannot exclude the possibility that the differences we see may reflect the limitations of our assay. Nevertheless, it strongly supports the need for further validation and exploration into distinguishing between the two mechanisms of repression.

Surprisingly, RE potency did not correlate with its ability to control Bcl10 binding or its ability to bind internally to other CARD11 domains. Though RE1 was the second strongest repressor, it had the greatest effect on Bcl10 association and intramolecular binding (Table 2.4, Figure 2.15 and Figure 2.16). To reconcile this difference, we propose that the specific repression of each RE is dictated by its intramolecular binding targets, whereby disruption to one domain has a greater effect on activity than disruption to another domain. Even so, because of the extremely weak binding of RE4 to other CARD11 domains, we could not determine its binding targets

and cannot claim that it has a unique target binding profile that accounts for its repressive potency. Therefore, we cannot eliminate alternative methods of RE repression.

There are multiple possible alternative methods of RE repression. One simple way is that the REs prevent association with an activating co-factor that is more correlative with NF- $\kappa$ B activity. It is not likely that this protein is a previously identified ID-regulated interactor of CARD11, such as MALT1, TRAF6, the IKK proteins, TAK1 or Caspase-8, because other hyperactive CARD11 variants did not spontaneously associate with them (Chan et al., 2013; Lamason et al., 2010). Candidate CARD11-interacting proteins that activate signaling that currently exist in the literature include ADAP, calmodulin-dependent protein kinase II (CaMKII), HPK1, aryl hydrocarbon receptor (AHR) interacting protein (AIP), stress-induced-phosphoprotein 1 homology and U-box containing protein 1 (STUB1) and Akt (Brenner et al., 2009; Cheng et al., 2014; Ishiguro et al., 2006; Medeiros et al., 2007; Narayan et al., 2006; Schimmack et al., 2014; Wang et al., 2013). Aside from preventing the association of these adaptors, the REs could associate with other proteins that inactivate the above signaling cofactors. These repressors may act by directly inhibiting CARD11 or other members of the signaling pathway. Potential negative regulator candidates include PP2A, PKC $\delta$  or casein kinase-2 interacting protein-1 (CKIP-1) (Eitelhuber et al., 2011; Liu et al., 2012; Sakamoto et al., 2014). Interestingly, CK1 $\alpha$  is a bifunctional regulator of CARD11-mediated signaling that requires the ID domain for binding (Bidere et al., 2009). In fact, CK1 $\alpha$  phosphorylation of S620 in RE4 was shown to be important for downregulating TCR signaling to NF- $\kappa$ B (Bidere et al., 2009). Because our M3 mutation includes S620 and

results in a modest affect on repression, it may support a partial contribution of CK1 $\alpha$  phosphorylation in RE4 repression. Therefore, it would be interesting to see if RE4 was sufficient to bind CK1 $\alpha$  and if CK1 $\alpha$  was necessary for RE4 repression.

We also report here the serendipitous discovery of two novel activating elements that were able to induce CARD11-mediated NF- $\kappa$ B activation to previously unappreciated levels (Figure 2.11). Despite limited similarity between the two AEs, both surprisingly share a PKC $\theta$  or PKC $\beta$  phosphorylation site (Matsumoto et al., 2005; Sommer et al., 2005). Both phosphorylation events have been shown to be triggered by lymphocyte stimulation and are required for downstream activation, but our studies may implicate a different role of these sites in the absence of Ag receptor engagement. Along these same lines, AE1 actually contains multiple serine and threonine residues that may contribute to the activating function. Some of these residues have previously been identified as phosphorylation sites after stimulation (Brenner et al., 2009; Matsumoto et al., 2005; Shinohara et al., 2007). So, it would be interesting to investigate their role in activation function as well. The outstanding question remains as to what role these AEs play in normal lymphocyte signaling. Why would these cells evolve the need to incur such robust activation? We anticipate this finding to open new and exciting avenues of studies into lymphocyte regulation.

The last functional element we identified, the inducibility element, was defined as the minimal region of the ID needed to induce NF- $\kappa$ B activation downstream of  $\alpha$ CD3 and  $\alpha$ CD28 signaling. This 25 amino acid element contains serine residues S563, S564, S567 and S577 previously implicated in activating downstream signaling (Brenner et al.,

2009; Matsumoto et al., 2005; Shinohara et al., 2007; Sommer et al., 2005).

Unexpectedly, we discovered that deletion of S649 and S657 had no effect on NF- $\kappa$ B signaling (Figure 2.2B). There is some controversy in the literature on the exact functions of these residues. With regards to S649, it was originally identified as a possible PKC $\theta$  substrate, but was dispensable for NF- $\kappa$ B activation downstream of PMA and  $\alpha$ CD3 (Matsumoto et al., 2005; Sommer et al., 2005). It was later detected by a phospho-S649-specific antibody after TCR stimulation and found to negatively regulate BCR stimulation independently of PKC $\beta$  (Moreno-Garcia et al., 2009). More recently, it was discovered that S649 is an Akt substrate (Cheng et al., 2014). When mutated by itself, S649 was activating, but when combined with S657, it cooperatively dampened NF- $\kappa$ B signaling (Cheng et al., 2014). This implies some interplay between S649 and S657 function and may explain why we see no effect of S649 deletion. The literature on S657 is more consistent as two groups identified it as a potential PKC $\theta$  substrate downstream of Ag receptor signaling that, when mutated, decreased NF- $\kappa$ B activation by about two fold (Matsumoto et al., 2005; Sommer et al., 2005). Our data contradicts their findings and necessitates further inquiries to resolve this discrepancy.

With seven regulatory elements encoded within the short 231 amino acids of the ID, we uncovered a highly modular method of controlling signaling output. We must now amend the previous, simple model of ID function by saying that CARD11 activity is determined by the interplay of all the functional elements. This includes all possible IE:AE, IE:RE, and AE:RE relationships. Future studies should reveal the nuances of these relationship, such as if IE neutralization completely abolishes RE function. If so, it

could reveal whether AEs require another regulatory step before becoming active. Our current data holds some clues about RE and AE relationships. For example, RE2 or RE3 was sufficient to completely repress AE2, but not could not fully repress AE1 and AE2 together (Figure 2.10B and Figure 2.14F), suggesting that different REs have different repressing potentials for each AE. One of the most intriguing relationships is the one between the IE and AE1 because the IE is completely embedded in AE1. It is unclear if the two elements utilize separate mechanisms to exert their functions. If they are not separable units, then does AE1 determine IE function or vice versa? Overall, we expect loss-of-function mutations in all seven elements would result in the activity levels of  $\Delta$ ID.

Finally, the discovery of redundant REs within the ID suggests that the ID is highly evolved to prevent the occurrence of spontaneous oncogenic mutations. This is especially important in light of the previously unappreciated potential for CARD11-mediated NF- $\kappa$ B activation (Figure 2.11B and Figure 2.13B). Even the most hyperactive lymphoma-associated CARD11 mutations are only about 10% as active as the quadruple RE mutant, suggesting that these variants are still considerably repressed (Chan et al., 2013; Lamason et al., 2010). The level of activation of several characterized CARD, LATCH and CC mutants was on par with the simultaneous mutations of two REs (Table 2.4). Our binding data is consistent with the notion that lymphoma-associated CARD11 mutation do not completely obstruct all RE function (Figure 2.19). Hence, we concluded that CARD11 point mutants only bypass some of the redundancy in REs by partially



disrupting binding to at least two REs. Furthermore, the RE redundancy provides a satisfying explanation for the lack of oncogenic mutations in the ID domain.

To our knowledge, this is the first study showing multiple functional elements within CARD11's inhibitory domain. It uncovers a highly modular mechanism of controlling both CARD11 and downstream Ag receptor activity. Furthermore, this may be the first in-depth characterization of an inhibitory domain whose activity is determined by so many regulatory components. It remains to be seen if this method of regulation is adopted by other ID-containing proteins or if this is specific to CARD11. Either way, our story adds a new facet to the already complex network of lymphocyte regulation and makes us appreciate just how well normal cells navigate through this regulatory landscape.

## References

- Bertin, J., Wang, L., Guo, Y., Jacobson, M.D., Poyet, J.L., Srinivasula, S.M., Merriam, S., DiStefano, P.S., and Alnemri, E.S. (2001). CARD11 and CARD14 are novel caspase recruitment domain (CARD)/membrane-associated guanylate kinase (MAGUK) family members that interact with BCL10 and activate NF-kappa B. *J. Biol. Chem.* *276*, 11877-11882.
- Bidere, N., Ngo, V.N., Lee, J., Collins, C., Zheng, L., Wan, F., Davis, R.E., Lenz, G., Anderson, D.E., Arnoult, D., *et al.* (2009). Casein kinase 1alpha governs antigen-receptor-induced NF-kappaB activation and human lymphoma cell survival. *Nature* *458*, 92-96.
- Brenner, D., Brechmann, M., Rohling, S., Tapernoux, M., Mock, T., Winter, D., Lehmann, W.D., Kiefer, F., Thome, M., Krammer, P.H., and Arnold, R. (2009). Phosphorylation of CARMA1 by HPK1 is critical for NF-kappaB activation in T cells. *Proc. Natl. Acad. Sci. U. S. A.* *106*, 14508-14513.
- Bu, R., Bavi, P., Abubaker, J., Jehan, Z., Al-Haqawi, W., Ajarim, D., Al-Dayel, F., Uddin, S., and Al-Kuraya, K.S. (2012). Role of nuclear factor-kappaB regulators TNFAIP3 and CARD11 in Middle Eastern diffuse large B-cell lymphoma. *Leuk. Lymphoma* *53*, 1971-1977.

- Chan, W., Schaffer, T.B., and Pomerantz, J.L. (2013). A quantitative signaling screen identifies CARD11 mutations in the CARD and LATCH domains that induce Bcl10 ubiquitination and human lymphoma cell survival. *Mol. Cell. Biol.* 33, 429-443.
- Che, T., You, Y., Wang, D., Tanner, M.J., Dixit, V.M., and Lin, X. (2004). MALT1/paracaspase is a signaling component downstream of CARMA1 and mediates T cell receptor-induced NF-kappaB activation. *J. Biol. Chem.* 279, 15870-15876.
- Cheng, J., Hamilton, K., and Kane, L. (2014). Phosphorylation of Carma1, but not Bcl10, by Akt regulates TCR/CD28-mediated NF- $\kappa$ B induction and cytokine production. *Mol Immunol.* 259, 110-116.
- Compagno, M., Lim, W.K., Grunn, A., Nandula, S.V., Brahmachary, M., Shen, Q., Bertoni, F., Ponzoni, M., Scandurra, M., Califano, A., *et al.* (2009). Mutations of multiple genes cause deregulation of NF-kappaB in diffuse large B-cell lymphoma. *Nature* 459, 717-721.
- Davis, R.E., Ngo, V.N., Lenz, G., Tolar, P., Young, R.M., Romesser, P.B., Kohlhammer, H., Lamy, L., Zhao, H., Yang, Y., *et al.* (2010). Chronic active B-cell-receptor signalling in diffuse large B-cell lymphoma. *Nature* 463, 88-92.
- Dong, G., Chanudet, E., Zeng, N., Appert, A., Chen, Y.W., Au, W.Y., Hamoudi, R.A., Watkins, A.J., Ye, H., Liu, H., *et al.* (2011). A20, ABIN-1/2, and CARD11

mutations and their prognostic value in gastrointestinal diffuse large B-cell lymphoma. *Clin. Cancer Res.* *17*, 1440-1451.

Egawa, T., Albrecht, B., Favier, B., Sunshine, M.J., Mirchandani, K., O'Brien, W., Thome, M., and Littman, D.R. (2003). Requirement for CARMA1 in antigen receptor-induced NF-kappa B activation and lymphocyte proliferation. *Curr. Biol.* *13*, 1252-1258.

Eitelhuber, A.C., Warth, S., Schimmack, G., Duwel, M., Hadian, K., Demski, K., Beisker, W., Shinohara, H., Kurosaki, T., Heissmeyer, V., and Krappmann, D. (2011). Dephosphorylation of Carma1 by PP2A negatively regulates T-cell activation. *EMBO J.* *30*, 594-605.

Gaide, O., Favier, B., Legler, D.F., Bonnet, D., Brissoni, B., Valitutti, S., Bron, C., Tschopp, J., and Thome, M. (2002). CARMA1 is a critical lipid raft-associated regulator of TCR-induced NF-kappa B activation. *Nat. Immunol.* *3*, 836-843.

Gaide, O., Martinon, F., Micheau, O., Bonnet, D., Thome, M., and Tschopp, J. (2001). Carma1, a CARD-containing binding partner of Bcl10, induces Bcl10 phosphorylation and NF-kappaB activation. *FEBS Lett.* *496*, 121-127.

Ishiguro, K., Green, T., Rapley, J., Wachtel, H., Giallourakis, C., Landry, A., Cao, Z., Lu, N., Takafumi, A., Goto, H., Daly, M.J., and Xavier, R.J. (2006). Ca<sup>2+</sup>/calmodulin-dependent protein kinase II is a modulator of CARMA1-mediated NF-kappaB activation. *Mol. Cell. Biol.* *26*, 5497-5508.

- Jun, J.E., Wilson, L.E., Vinuesa, C.G., Lesage, S., Blery, M., Miosge, L.A., Cook, M.C., Kucharska, E.M., Hara, H., Penninger, J.M., *et al.* (2003). Identifying the MAGUK protein Carma-1 as a central regulator of humoral immune responses and atopy by genome-wide mouse mutagenesis. *Immunity* *18*, 751-762.
- Lamason, R.L., McCully, R.R., Lew, S.M., and Pomerantz, J.L. (2010). Oncogenic CARD11 mutations induce hyperactive signaling by disrupting autoinhibition by the PKC-responsive inhibitory domain. *Biochemistry* *49*, 8240-8250.
- Lenz, G., Davis, R.E., Ngo, V.N., Lam, L., George, T.C., Wright, G.W., Dave, S.S., Zhao, H., Xu, W., Rosenwald, A., *et al.* (2008). Oncogenic CARD11 mutations in human diffuse large B cell lymphoma. *Science* *319*, 1676-1679.
- Li, Y., Spangenberg, O., Paarmann, I., Konrad, M., and Lavie, A. (2002). Structural basis for nucleotide-dependent regulation of membrane-associated guanylate kinase-like domains. *J. Biol. Chem.* *277*, 4159-4165.
- Liu, Y., Song, R., Gao, Y., Li, Y., Wang, S., Liu, H.Y., Wang, Y., Hu, Y.H., and Shu, H.B. (2012). Protein kinase C-delta negatively regulates T cell receptor-induced NF-kappaB activation by inhibiting the assembly of CARMA1 signalosome. *J. Biol. Chem.* *287*, 20081-20087.
- Lohr, J.G., Stojanov, P., Lawrence, M.S., Auclair, D., Chapuy, B., Sougnez, C., Cruz-Gordillo, P., Knoechel, B., Asmann, Y.W., Slager, S.L., *et al.* (2012). Discovery and prioritization of somatic mutations in diffuse large B-cell lymphoma (DLBCL) by

whole-exome sequencing. *Proceedings of the National Academy of Sciences* *109*, 3879-3884.

Matsumoto, R., Wang, D., Blonska, M., Li, H., Kobayashi, M., Pappu, B., Chen, Y., Wang, D., and Lin, X. (2005). Phosphorylation of CARMA1 plays a critical role in T Cell receptor-mediated NF-kappaB activation. *Immunity* *23*, 575-585.

McCully, R.R., and Pomerantz, J.L. (2008). The protein kinase C-responsive inhibitory domain of CARD11 functions in NF-kappaB activation to regulate the association of multiple signaling cofactors that differentially depend on Bcl10 and MALTI for association. *Mol. Cell. Biol.* *28*, 5668-5686.

McGee, A.W., and Bredt, D.S. (1999). Identification of an intramolecular interaction between the SH3 and guanylate kinase domains of PSD-95. *J. Biol. Chem.* *274*, 17431-17436.

Medeiros, R.B., Burbach, B.J., Mueller, K.L., Srivastava, R., Moon, J.J., Highfill, S., Peterson, E.J., and Shimizu, Y. (2007). Regulation of NF-kappaB activation in T cells via association of the adapter proteins ADAP and CARMA1. *Science* *316*, 754-758.

Montesinos-Rongen, M., Schmitz, R., Brunn, A., Gesk, S., Richter, J., Hong, K., Wiestler, O.D., Siebert, R., Kupperts, R., and Deckert, M. (2010). Mutations of CARD11 but not TNFAIP3 may activate the NF-kappaB pathway in primary CNS lymphoma. *Acta Neuropathol.* *120*, 529-535.

- Moreno-Garcia, M.E., Sommer, K., Haftmann, C., Sontheimer, C., Andrews, S.F., and Rawlings, D.J. (2009). Serine 649 phosphorylation within the protein kinase C-regulated domain down-regulates CARMA1 activity in lymphocytes. *J. Immunol.* *183*, 7362-7370.
- Narayan, P., Holt, B., Tosti, R., and Kane, L.P. (2006). CARMA1 is required for Akt-mediated NF-kappaB activation in T cells. *Mol. Cell. Biol.* *26*, 2327-2336.
- Oliva, C., Escobedo, P., Astorga, C., Molina, C., and Sierralta, J. (2012). Role of the maguk protein family in synapse formation and function. *Developmental Neurobiology* *72*, 57-72.
- Pan, L., Chen, J., Yu, J., Yu, H., and Zhang, M. (2011). The structure of the PDZ3-SH3-GuK tandem of ZO-1 protein suggests a supramodular organization of the membrane-associated guanylate kinase (MAGUK) family scaffold protein core. *J. Biol. Chem.* *286*, 40069-40074.
- Pomerantz, J.L., Denny, E.M., and Baltimore, D. (2002). CARD11 mediates factor-specific activation of NF-kappaB by the T cell receptor complex. *EMBO J.* *21*, 5184-5194.
- Qian, Y., and Prehoda, K.E. (2006). Interdomain interactions in the tumor suppressor discs large regulate binding to the synaptic protein GukHolder. *J. Biol. Chem.* *281*, 35757-35763.

- Sakamoto, T., Kobayashi, M., Tada, K., Shinohara, M., Io, K., Nagata, K., Iwai, F., Takiuchi, Y., Arai, Y., Yamashita, K., *et al.* (2014). CKIP-1 is an intrinsic negative regulator of T-cell activation through an interaction with CARMA1. *PLoS One* *9*, e85762.
- Schimmack, G., Eitelhuber, A.C., Vincendeau, M., Demski, K., Shinohara, H., Kurosaki, T., and Krappmann, D. (2014). AIP augments CARMA1-BCL10-MALT1 complex formation to facilitate NF-kappaB signaling upon T cell activation. *Cell. Commun. Signal.* *12*, 49-014-0049-7.
- Schulze-Luehrmann, J., and Ghosh, S. (2006). Antigen-receptor signaling to nuclear factor kappa B. *Immunity* *25*, 701-715.
- Shinohara, H., Maeda, S., Watarai, H., and Kurosaki, T. (2007). IkappaB kinase beta-induced phosphorylation of CARMA1 contributes to CARMA1 Bcl10 MALT1 complex formation in B cells. *J. Exp. Med.* *204*, 3285-3293.
- Shinohara, H., Yasuda, T., Aiba, Y., Sanjo, H., Hamadate, M., Watarai, H., Sakurai, H., and Kurosaki, T. (2005). PKC beta regulates BCR-mediated IKK activation by facilitating the interaction between TAK1 and CARMA1. *J. Exp. Med.* *202*, 1423-1431.
- Sommer, K., Guo, B., Pomerantz, J.L., Bandaranayake, A.D., Moreno-Garcia, M.E., Ovechkina, Y.L., and Rawlings, D.J. (2005). Phosphorylation of the CARMA1 linker controls NF-kappaB activation. *Immunity* *23*, 561-574.



- Wang, D., You, Y., Case, S.M., McAllister-Lucas, L.M., Wang, L., DiStefano, P.S., Nunez, G., Bertin, J., and Lin, X. (2002). A requirement for CARMA1 in TCR-induced NF-kappa B activation. *Nat. Immunol.* 3, 830-835.
- Wang, S., Li, Y., Hu, Y.H., Song, R., Gao, Y., Liu, H.Y., Shu, H.B., and Liu, Y. (2013). STUB1 is essential for T-cell activation by ubiquitinating CARMA1. *Eur. J. Immunol.* 43, 1034-1041.
- Wegener, E., and Krappmann, D. (2007). CARD-Bcl10-Malt1 signalosomes: missing link to NF-kappaB. *Sci. STKE* 2007, pe21.
- Wegener, E., Oeckinghaus, A., Papadopoulou, N., Lavitas, L., Schmidt-Supprian, M., Ferch, U., Mak, T.W., Ruland, J., Heissmeyer, V., and Krappmann, D. (2006). Essential role for IkappaB kinase beta in remodeling Carma1-Bcl10-Malt1 complexes upon T cell activation. *Mol. Cell* 23, 13-23.

## Curriculum Vitae

### CURRICULUM VITAE FOR Ph.D. CANDIDATES

The Johns Hopkins University School of Medicine

**Rakhi P. Jattani**

December 2014

#### **Educational History**

Ph.D. expected	2014	Program in Biochemistry, Cell and Molecular Biology Johns Hopkins School of Medicine Mentor: Joel L. Pomerantz, Ph.D.
B.S.	2004	Biological Sciences Carnegie Mellon University, Mellon College of Science

#### **Other Professional Experience**

Research Rotation	2006	Lab of Dr. Geraldine Seydoux Johns Hopkins School of Medicine
Research Rotation	2006	Lab of Dr. Jef Boeke Johns Hopkins School of Medicine
Research Technician	2004 – 2006	Lab of Dr. Monn Monn Myat Weill Medical College of Cornell University
Student Research Assistant	2002 – 2004	Lab of Dr. Javier López Carnegie Mellon University
Undergraduate Research Fellow	2003	Lab of Dr. Michael Young Rockefeller University

#### **Scholarships and Fellowships**

2002 – 2004	Maxwell H. and Gloria Connan Scholarship Undergraduate scholarship
2003	Summer Undergraduate Research Fellowship Direct cost: \$2,500 PI: Michael Young, Rockefeller University, New York, NY Role/effort: Undergraduate researcher/100%
2002	Summer Undergraduate Research Program Direct cost: \$3,000 PI: Javier López, Carnegie Mellon University, Pittsburgh, PA Role/effort: Undergraduate researcher/100%

### **Honors & Awards**

2011 Finalist, Johns Hopkins University Biotechnology Case Competition  
2004 University Honors, Carnegie Mellon University  
2001 – 2004 Dean's List

### **Publications**

**Jattani R**, Patel U, Kerman B, Myat MM. (2009) Deficiency screen identifies a novel role for beta 2 tubulin in salivary gland and myoblast migration in the *Drosophila* embryo. *Developmental Dynamics* **238**, 853-63. PMID: PMC3105526.

Pirraglia C, **Jattani R**, Myat MM. (2006) Rac function in epithelial tube morphogenesis. *Developmental Biology* **290**, 435-45.

### **Meetings and Presentations**

**Jattani, R.** and Myat, MM. (2006)  $\beta$ -tubulin 85D is Required for Cell Shape Changes during Embryonic Salivary Gland Development. 47<sup>th</sup> Annual Drosophila Research Conference. Houston, TX. Poster Presentation, March 2006.

### **Service and Leadership**

2013 – 2014 Director of Events, Johns Hopkins Business and Consulting Club  
2010 – 2014 Graduate Rotation Student Mentor  
2010 – 2014 Workshop Coordinator, Johns Hopkins University Community Science Day